

PATTERN RECONFIGURABLE METAMATERIAL ANTENNA FOR 5G BASE STATION NETWORK

BASHAR ALI FAREA ESMAIL



UNIVERSITI TUN HUSSEIN ONN MALAYSIA

UNIVERSITI TUN HUSSEIN ONN MALAYSIA

STATUS CONFIRMATION FOR THESIS
DOCTOR OF PHILOSOPHY

PATTERN RECONFIGURABLE METAMATERIAL ANTENNA FOR 5G
BASE STATION NETWORK

ACADEMIC SESSION: 2020/2021

I, **BASHAR ALI FAREA ESMAIL**, agree to allow this Doctoral Thesis to be kept at the Library under the following terms:

1. This Doctoral Thesis is the property of the Universiti Tun Hussein Onn Malaysia.
2. The library has the right to make copies for educational purposes only.
3. The library is allowed to make copies of this report for educational exchange between higher educational institutions.
4. The library is allowed to make available full text access of the digital copy via the internet by Universiti Tun Hussein Onn Malaysia in downloadable format provided that the Thesis is not subject to an embargo. Should an embargo be in place, the digital copy will only be made available as set out above once the embargo has expired
5. ** Please Mark (✓)

☐

CONFIDENTIAL

(Contains information of high security or of great importance to Malaysia as STIPULATED under the OFFICIAL SECRET ACT 1972) *Title and Abstract only*

☐

RESTRICTED

(Contains restricted information as determined by the organization/ institution where research was conducted) *Title, Abstract and introduction only*

☐

EMBARGO _____ until _____
(date) (date)

☒

FREE ACCESS



BASHAR ALI FAREA ESMAIL

Permanent address:

AL-MOUHAFADAH STREET, IBB
CITY, 1119, YEMEN.

Date: 31/1/2021

Approved by,



DR. HUDA BIN A. MAJID

NOTE:

** If this Doctoral Thesis classified as CONFIDENTIAL or RESTRICTED, please attach the letter from the relevant authority/organization stating reasons and duration for such classifications.

This thesis has been examined on August 23, 2020
and is sufficient in fulfilling the scope and quality for the purpose of awarding the
Degree of Doctor of Philosophy in Electrical Engineering.

Chairperson:

ASSOC. PROF. DR. TAY KIM GAIK
Faculty of Electrical & Electronic Engineering
Universiti Tun Hussein Onn Malaysia

Examiners:

PROF. DR. ZAHRILADA ZAKARIA
Faculty of Electronic and Computer Engineering
Universiti Teknikal Malaysia Melaka

ASSOC. PROF. DR. KHAIRUN NIDZAM BIN RAMLI
Faculty of Electrical & Electronic Engineering
Universiti Tun Hussein Onn Malaysia



PATTERN RECONFIGURABLE METAMATERIAL ANTENNA FOR 5G BASE
STATION NETWORK

BASHAR ALI FAREA ESMAIL

A thesis submitted in
fulfillment of the requirement for the award of the
Doctor of Philosophy in Electrical Engineering



Faculty of Electrical and Electronic Engineering
Universiti Tun Hussein Onn Malaysia

JANUARY 2021

I hereby declare that the work in this thesis is my own except for quotations and summaries which have been duly acknowledged.

Student : 

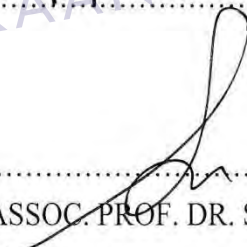
BASHAR ALI FAREA ESMAIL

Date : 3/1/2021

Supervisor : 

DR. HUDA BIN A. MAJID

Date : 3/1/2021

Co-supervisor : 

ASSOC. PROF. DR. SAMSUL HAIMI BIN DAHLAN

Date : 4/1/2021



PTT ALUTHM
PERPUSTAKAAN TUN AMINAH

Sincerely dedicated to my beloved Mother and Father...



PTTA UTHM
PERPUSTAKAAN TUNKU TUN AMINAH

ACKNOWLEDGEMENT

Deep and humble gratitude to ALLAH Almighty for providing the opportunity and giving me the strength to complete this work.

My profound gratitude goes to my supervisor Dr. Huda Bin A. Majid, for his invaluable guidance, excellent supervision, continuous encouragement and constant support in making this research possible. His cooperation, tolerance, constructive criticism and useful suggestions have been of immense encouragement to me and enabled me to develop a deeper understanding of this research. I am also grateful to my co-supervisor Assoc. Prof. Dr. Samsul Haimi Bin Dahlan and Prof. Dr. Mohamed Himdi for their cooperative support during the entire period of this research.

I am especially indebted to my parents, who were my first teachers in this world by setting a good example for me about how to live, study, work and for their love, sacrifices, and support. I also acknowledge with thanks and humility my wife and daughters who have remained my anchor in terms of love, support, encouragement and prayers. I will forever remain grateful to them.

Finally, I extend my gratitude to all those who were directly or indirectly involved by either encouraging, praying or offering constructive advice in this work.



ABSTRACT

Reconfiguration of an antenna's radiation pattern in a predefined direction is very important for enhancing the performance of communication systems in terms of the quality of service, system security, avoiding interference, and economizing power. Metamaterials, on the other hand, are commonly used in antenna design to enhance the gain, bandwidth, and efficiency and recently to tilt the radiation beam. Nonetheless, few issues had been encountered especially when the frequency is pushed to higher range such as the inherent losses that restrict the variety of their applications. Hence, metamaterials structures with relatively low loss are in high demand. In this thesis, various metamaterial structures with low loss properties are proposed. Then these structures are reconfigured and integrated with the fifth-generation (5G) planar antennas at two different frequency bands i.e. millimetre-wave (MMW) band and sub-6 GHz band for beam deflection applications. The modified double square ring resonator (DSRR) and contiguous squares resonator (CSR) structures are investigated numerically and experimentally to provide low loss property at 76 GHz and around 28 GHz, respectively. DSRR and CSR achieve losses of 0.5 dB and 0.2 dB, respectively. Both structures are manufactured and measured to validate the results. Furthermore, the analytical model is introduced to predict the electromagnetic behaviour of the proposed metamaterial structures. Thereafter, the CSR, Bridge shaped resonator (BSR) and split square resonator (SSR) structures are electronically reconfigured to produce different refractive indices at MMW and sub-6 GHz spectrums, which are used for deflecting the radiation beam of the 5G planar antennas. An array of unreconfigurable adjacent square-shaped resonators (ASSRs) has been also used for tilting the radiation pattern of planar antenna at sub-6 GHz spectrum. These proposed structures are included in the substrate of the dipole antenna and bow-tie antenna for deflecting the radiation pattern in E-plane at two different 5G bands of 28 GHz and 3.5 GHz. The results of all designs at both bands show that the radiation beam of the antennas is deflected in both positive and negative directions with respect to y-direction of antenna. At 28 GHz, a high

deflection angle of 34° is obtained using simple structure, BSR, with gain improvement up to 1.9 dB (26.7%). On the other hand, at 3.5 GHz, the beam deflection angle of $\pm 39^\circ$ is achieved with gain enhancement up to 2.4 dB (35.6%) using passive beam deflection antenna whereas the beam deflection of $\pm 36^\circ$ is obtained using an active beam deflection antenna. The reconfigurable metamaterial antennas are proposed to be used in 5G base station network with advantages of high deflection angles, gain enhancement, low profile structure, low cost, lightweight, and easy integration with other circuits for 5G beam deflection applications.



PTTA UTHM
PERPUSTAKAAN TUNKU TUN AMINAH

ABSTRAK

Corak radiasi bagi konfigurasi semula antenna dalam arah yang ditetapkan adalah sangat penting untuk meningkatkan prestasi sistem komunikasi dari segi kualiti perkhidmatan, keselamatan sistem, mengelakkan gangguan dan menjimatkan kuasa. Selain itu, bahanmeta, kebiasaanya digunakan dalam reka bentuk antenna untuk meningkatkan gandaan, jalur lebar, dan kecekapan dan kebelakangan ini untuk mencondongkan alur radiasi. Walau bagaimanapun, beberapa isu telah ditemui khususnya apabila frekuensi ditolak kepada julat yang lebih tinggi iaitu seperti kehilangan terwujud yang menyekat pelbagai aplikasi. Oleh itu, struktur bahanmeta dengan kehilangan yang rendah berada dalam permintaan tinggi. Dalam tesis ini, pelbagai struktur bahanmeta diperkenalkan dengan sifat kehilangan yang rendah. Kemudian, struktur ini dikonfigurasi semula dan diintegrasikan dengan antenna satahan generasi kelima (5G) pada dua jalur frekuensi yang berbeza iaitu jalur gelombang-milimeter (MMW) dan pecahan-6 GHz untuk aplikasi alur pesongan. Struktur resonator dua cincin segiempat terubahsuai dan struktur resonator segi empat bersebelahan disiasat secara numerik dan eksperimen untuk menyediakan sifat kehilangan masing-masing pada 76 GHz dan sekitar 28 GHz. Masing-masing DSRR dan CSR mencapai kehilangan rendah sebanyak 0.5 dB dan 0.2 dB. Kedua-dua struktur dihasilkan dan diukur untuk mengesahkan keputusan. Selanjutnya, model analitikal diperkenalkan untuk meramalkan kelakuan elektromagnetik bagi struktur bahanmeta yang dicadangkan. Sesudah itu, struktur CSR, struktur resonator berbentuk penghubung (BSR) dan resonator empat segi bersela (SRR) telah dikonfigurasi secara elektronik untuk menghasilkan indeks biasan yang berlainan pada spektrum MMW dan pecahan-6 GHz, yang digunakan untuk memesongkan alur radiasi antenna satahan 5G. Aturan resonator berbentuk segi empat bersebelahan (ASSR) yang tidak dikonfigurasi juga telah digunakan untuk mencondongkan corak radiasi antenna satahan di spektrum pecahan-6 GHz. Struktur yang dicadangkan ini dirangkumi dalam substrat antenna dwikutub dan antenna tali leher bow untuk memesongkan corak sinaran dalam satah E pada dua jalur 5G yang berbeza pada 28

GHz dan 3.5 GHz. Keputusan semua reka bentuk pada kedua-dua jalur ini menunjukkan bahawa alur radiasi antenna dibelokkan dalam kedua-dua arah positif dan negatif berkenaan dengan arah y antenna. Pada 28 GHz, sudut pesongan tinggi 34° diperoleh menggunakan struktur sederhana, BSR, dengan peningkatan keuntungan hingga 1.9 dB (26.7%). Sebaliknya, pada 3.5 GHz, sudut pesongan pancaran $\pm 39^\circ$ achieved dicapai dengan peningkatan kenaikan hingga 2.4 dB (35.6%) menggunakan antenna pesongan sinar pasif sedangkan pesongan sinar $\pm 36^\circ$ diperoleh menggunakan antenna pesongan sinar aktif. Antena metamaterial yang boleh dikonfigurasi semula dicadangkan untuk digunakan dalam rangkaian stesen pangkalan 5G dengan kelebihan sudut pesongan tinggi, peningkatan keuntungan, struktur profil rendah, kos rendah, ringan, dan penyatuan mudah dengan litar lain untuk aplikasi pesongan sinar 5G.



CONTENTS

TITLE	i
DECLARATION	ii
DEDICATION	iii
ACKNOWLEDGEMENT	iv
ABSTRACT	v
ABSTRAK	vii
CONTENTS	ix
LIST OF TABLES	xiv
LIST OF FIGURES	xvi
LIST OF SYMBOLS AND ABBREVIATION	xxvi
LIST OF APPENDICES	xxviii
CHAPTER 1 INTRODUCTION	1
1.1 Introduction	1
1.2 Motivation	4
1.3 Problem statement	5
1.4 Objectives	6
1.5 Scopes of the research	7
1.6 Research structure outline	8
CHAPTER 2 LITERATURE REVIEW	11
2.1 Introduction	11
2.2 Metamaterials	13
2.2.1 History	13
2.2.2 Metamaterial applications	14
2.2.3 Metamaterial classifications	14
2.2.4 Refractive index of the metamaterials	16



2.3	Metamaterial loss	17
2.3.1	Electromagnetically induced transparency (EIT) technique	19
2.3.2	Tailoring geometry of metamaterials	22
2.4	Reconfigurable metamaterials	25
2.4.1	Electronically reconfigurable metamaterials	25
2.4.2	Applications of reconfigurable metamaterials	27
2.5	MMW spectrum for future 5G communications	27
2.6	Reconfigurable antenna	29
2.6.1	Frequency reconfigurable antenna	29
2.6.2	Polarization reconfigurable antenna	30
2.6.3	Radiation pattern reconfigurable antenna	30
2.6.3.1	Antenna loaded by metamaterials for beam deflection applications	32
2.7	Chapter summary	37
CHAPTER 3	RESEARCH METHODOLOGY	38
3.1	Introduction	38
3.2	Methodology	41
3.2.1	Design and simulation	41
3.2.1.1	The design and boundary conditions for the simulation setup	41
3.2.1.2	Retrieve the constitutive parameters	42
3.2.1.3	PIN diode	43
3.2.1.4	The simulation steps	45
3.2.1.5	Analysis of the metamaterial structures	48
3.2.1.6	Metamaterial equivalent circuit model	49
3.2.1.7	Antenna design	52



3.2.1.8	Beam deflection antenna approaches	54
3.2.2	Fabrication and measurement	56
3.2.2.1	Fabrication Process	56
3.2.2.2	Fabrication and measurement of metamaterial structures	59
3.2.2.3	Measurement of metamaterial Antenna	61
3.3	Chapter summary	63
CHAPTER 4	METAMATERIAL STRUCTURES	64
4.1	Metamaterial structure at MMW regime	65
4.1.1	Modified double square ring resonator (DSRR)	65
4.1.1.1	Equivalent circuit of the DSRR structure	66
4.1.1.2	DSRR performance analysis	67
4.1.1.3	Experimental validation	69
4.1.2	Contiguous squares resonator (CSR)	71
4.1.2.1	Equivalent circuit of the CSR structure	73
4.1.2.2	CSR performance analysis	74
4.1.2.3	Experimental validation	76
4.1.2.4	Reconfigurable CSR structure	77
4.1.2.4.1	Copper strip simulation method	78
4.1.2.4.2	S-Parameters simulation method	80
4.1.3	Bridge shape resonator (BSR)	82
4.1.3.1	Equivalent circuit of the BSR structure	83
4.1.3.2	BSR performance analysis	84
4.1.3.3	Reconfigurable BSR structure	87
4.2	Metamaterial structures at microwave regime	89



4.2.1	Adjacent square-shaped resonator (ASSR)	89
4.2.1.1	ASSR performance analysis	90
4.2.2	Split square resonator (SSR)	92
4.2.2.1	Equivalent circuit of the SSR structure	93
4.2.2.2	Reconfigurable the SSR Structure using copper strip	95
4.2.2.3	Reconfigurable the SSR Structure using s-parameters	97
4.3	Chapter summary	100
CHAPTER 5	5G BEAM DEFLECTION ANTENNA AT 28 GHZ	101
5.1	Printed dipole antenna design	101
5.1.1	Experimental validation of designed prototype	105
5.1.2	Antenna loaded by CSR array	107
5.1.2.1	Theoretical analysis of beam deflection	107
5.1.2.2	The performance of the antenna loaded by CSR array	109
5.1.3	Antenna loaded by BSR array	118
5.2	Chapter summary	127
CHAPTER 6	5G BEAM DEFLECTION ANTENNA AT 3.5 GHZ MICROWAVE BAND	128
6.1	Design of dipole antenna	128
6.1.1	Theoretical concept of beam deflection	130
6.1.2	Antenna loaded ASSR structure	131
6.2	Design of bow-tie antenna	138
6.2.1	Simulation results and experimental validation of designed prototype	140
6.2.2	The performance of the antenna in the presence of SRR array	142



6.2.2.1	Theoretical analysis of beam deflection	142
6.2.2.2	Passive beam deflection antenna	143
6.2.2.3	Active beam deflection antenna	150
6.3	Chapter summary	158
CHAPTER 7	CONCLUSIONS AND FUTURE WORK	159
7.1	Conclusion	159
7.1.1	Low loss metamaterials	159
7.1.2	Reconfigurable metamaterial structures	160
7.1.3	Beam deflection antenna using metamaterials	161
7.2	Key contribution	162
7.3	Future work	164
REFERENCES		165
APPENDICES		177



PTTAUTHM
PERPUSTAKAAN TUNKU TUN AMINAH

LIST OF TABLES

2.1	Summary of previous reports on metamaterial loss reduction	23
2.2	Characteristics comparison of the switching components	26
2.3	Beam deflection antenna loaded by metamaterial structure	34
3.1	The prior design specifications of the printed dipole and bow-tie antennas	53
4.1	CSR unit cell geometrical dimensions	72
4.2	Calculated values of the circuit components	74
4.3	Switches configurations, resonance frequencies and refractive index of the reconfigurable CSR structure	82
4.4	The dimensions of the BSR structure	83
4.5	Calculated values of the circuit components	84
4.6	Geometry specifications of the proposed metamaterial structure	90
4.7	SSR unit cell geometrical dimensions	93
4.8	Comparison of the present works with that reported literature for metamaterial loss reduction	98
5.1	Geometric specifications of the printed dipole antenna	103
5.2	Comparison of the present works with that reported literature for beam deflection antenna using metamaterial	126
6.1	Geometrical specifications of the proposed antenna	130
6.2	The impact of increasing of unit cells on the beam deflection and the antenna gain (negative tilt angle)	134
6.3	Effect of the number of unit cells on the beam	

	deflection and the antenna gain (positive tilt angle)	138
6.4	Geometrical dimensions of the proposed antenna	140
6.5	Comparison of the performance of the reconfigurable antenna using PIN diodes	151
6.6	Comparison of the present works with that reported literature for beam deflection antenna using metamaterial	157



PTTA UTHM
PERPUSTAKAAN TUNKU TUN AMINAH

LIST OF FIGURES

1.1	The steps of the thesis outline	9
2.1	Conventional array of metamaterials, TW structure exhibits ($-\epsilon$) and SRR provides ($-\mu$)	14
2.2	Classifications of the mediums based on permittivity and permeability with the electromagnetic wave interacting with four possible materials	15
2.3	The inherent losses in metamaterials	18
2.4	Schematic view of the structure and the fabricated prototype	20
2.5	(a) Schematic view of SRRs and cut wire, and (b) simulated and measured transmission and reflection coefficients	20
2.6	(a) The periodic structure with a single unit cell geometry, and (b) simulated and measured transmission and reflection coefficients	21
2.7	(a) Schematic view of SRRs and I-shape cut wire, and (b) fabricated prototype	22
2.8	Average atmospheric attenuation of MMW	28
3.1	Flow chart of the research	39
3.2	Design process of the low loss metamaterial and reconfigurable metamaterial antenna	40
3.3	Robust retrieve method steps	42
3.4	Circuit diagram of the PIN diode when (a) ON state and (b) OFF state	44
3.5	PIN diode structure of the MA4AGFCP910 ($A= 0.6$ mm and $B= 0.36$ mm) and BAR50-02V ($A= 1$ mm and $B= 0.6$ mm)	44

3.6	Two operation modes of the MA4AGFCP910 diode (a) ON (forward bias), and (b) OFF (reverse bias)	45
3.7	Two operation modes of the of the BAR50-02V diode (a) ON (forward bias), and (b) OFF (reverse bias)	45
3.8	Copper strip to mimic the PIN diode dimension (a) vacuum to represent OFF state (b) copper strip to represent ON state	46
3.9	Metamaterial unit cell	46
3.10	Discrete port	47
3.11	Schematic window in CST software	47
3.12	Beam deflection antenna using reconfigurable metamaterial	48
3.13	Rectangular conducting strip with the length ℓ_s and width w_s	50
3.14	Two parallel strips on the top of substrate layer	51
3.15	Biased circuit of the bow-tie antenna loading by SSR unit cells	54
3.16	Laminator machine	56
3.17	The ultra-violet (UV) light machine	57
3.18	Etching machine	57
3.19	8330S-21G silver conductive epoxy glue	58
3.20	The glue parts with 1:1 mix ratio	58
3.21	Installation of the diode at the gap of the structure	59
3.22	The setup of the S parameters measurement (a) layout and (b) equipment used in the measurement	60
3.23	Reflection coefficient measurement (a) at MMW spectrum and (b) Sub-6 GHz	61
3.24	Layout of radiation pattern measurement	62
3.25	Radiation pattern measurement setup	62
4.1	DSRRs periodic array with the geometrical arrangement of the unit cell	65
4.2	Equivalent circuit of the DSRR metamaterial structure	66
4.3	The reflection and transmission coefficients of the	



simulation and equivalent circuit model of the DSRR metamaterial	67
4.4 Induced surface current of the proposed unit cell at 76 GHz a) Front view b) back view	68
4.5 (a) The front view of the fabricated DSRRs periodic structure (6 x 7 array), (b) microscopic structure of the MDSRR prototype, and (c) waveguide loaded with DSRRs periodic structure	69
4.6 The reflection and transmission coefficients of the simulated and measured results of the DSRR metamaterial	70
4.7 Real refractive index of the simulated and measured results of the DSRR metamaterial structure	71
4.8 Schematic view of the CSR periodic structure and the geometry of the single unit cell	72
4.9 (a) The simulated surface current of CSR structure and (b) Equivalent circuit of CSR structure	73
4.10 The S-parameters of the CSR structure	74
4.11 Prototype of the CSR periodic structure	76
4.12 Simulated and measured S-parameters results of the proposed metamaterial structure	76
4.13 Real refractive index of the CSR metamaterial structure	77
4.14 Reconfigurable metamaterial structure using three diodes	78
4.15 Figure 4.15: Reconfigurable CSR using copper strip (a) OFF state and (b) ON state	78
4.16 The reflection and transmission coefficients of the reconfigurable CSR structure	79
4.17 Real parts of the refractive index of the reconfigurable metamaterial structure	79
4.18 Circuit simulation using CST software a) On state b) OFF state	80

4.19	Reflection and transmission coefficients of the reconfigurable CSR structure	81
4.20	Real parts of the refractive index of the reconfigurable metamaterial structure	81
4.21	Schematic view of the BSR structure	82
4.22	Equivalent circuit model of the BSR metamaterial structure	83
4.23	Reflection and transmission coefficients of the proposed BSR	85
4.24	Real refractive index of the BSR structure	86
4.25	Reconfigurable metamaterial structure using four PIN diodes	87
4.26	The reflection and transmission coefficients of the reconfigurable BSR structure	87
4.27	Real refractive index of the reconfigurable BSR structure	88
4.28	ASSR structure (a) the designed configuration, (b) equivalent circuit	89
4.29	Simulated and equivalent circuit S-parameters results of the proposed ASSR structure	91
4.30	The reconstructed refractive index of the proposed ASSR structure	92
4.31	Schematic view of the split square resonator (SSR)	92
4.32	The equivalent circuit of the proposed SSR structure	93
4.33	The simulation and equivalent circuit results of the S-parameters of the proposed SSR structure	94
4.34	Reconfigurable the metamaterial structure	95
4.35	The reflection and transmission coefficients of the reconfigurable metamaterial	96
4.36	The retrieved refractive indices of the reconfigurable SSR structure	96
4.37	The reflection and transmission coefficients of the reconfigurable metamaterial using S-parameters	97



4.38	The retrieved refractive indices of the reconfigurable SSR	97
5.1	The printed dipole antenna (a) and (b) the front and back layers of the designed configuration, (c) and (d) the front and back layers of the fabricated prototype	103
5.2	Reflection coefficient of the printed dipole antenna	104
5.3	Normalized radiation patterns of the proposed antenna (a) E-plane (b) H-plane	104
5.4	Electric field distribution of the antenna in E-plane at 28 GHz	105
5.5	Radiation power flow (Poynting vector) of the proposed antenna in E-plane at 28 GHz	105
5.6	Measured and simulated reflection coefficient of the printed dipole antenna	106
5.7	Measured and simulated radiation patterns of the printed dipole antenna (a) E-plane (b) H-plane	106
5.8	(a) Two metamaterial configurations with their dimensions on xy-plane (b) electromagnetic ray routes and their locations from the feed point in the coordinate plane for array factor and radiation pattern calculations	107
5.9	The antenna radiation pattern when loaded by reconfigurable metamaterial	109
5.10	Dipole antenna with 2×3 CSR unit cells for positive deflection (a) the designed configuration and (b) fabricated prototype	109
5.11	The reflection coefficient of the simulation and measurement of the dipole antenna with and without CSR during the positive deflection	110
5.12	Normalized results of simulation and measurement radiation patterns of the dipole antenna with metamaterial array in E-plane at (a) 27.7 GHz, (b) 28 GHz, (c) 28.3 GHz d) in H-plane at 28 GHz	111



5.13	Gain results of the simulation and measurement of the proposed antenna with and without metamaterial array for positive deflection at 28 GHz	112
5.14	Radiation power flow (Poynting vector) of the dipole antenna in E-plane at 28 GHz (a) without metamaterial unit cells (b) with metamaterial unit cells	113
5.15	Dipole antenna with 2×3 metamaterial unit cells for negative deflection, (a) designed configuration and (b) fabricated prototype	113
5.16	The reflection coefficient of the simulation and measurement of the dipole antenna with and without metamaterial unit cells during the negative deflection	114
5.17	Simulated and measured normalized radiation patterns of the dipole antenna with metamaterial array in E-plane at (a) 27.7 GHz (b) 28 GHz (c) 28.3 GHz and d) in H-plane at 28 GHz	115
5.18	Gain results of the simulation and measurement of the proposed antenna with and without metamaterial array for negative deflection at 28 GHz	116
5.19	Radiation power flow (Poynting vector) of the dipole antenna in E-plane at 28 GHz (a) without metamaterial unit cells (b) with metamaterial unit cells	116
5.20	Dipole antenna with 2×3 metamaterial unit cells for zero deflection (a) designed configuration and (b) fabricated prototype	117
5.21	Simulated and measured reflection coefficient of the dipole antenna with metamaterial unit cells at zero deflection angle	118
5.22	Simulated and measured normalized radiation patterns of the dipole antenna with metamaterial array at 28 GHz (a) E-plane (b) H-plane	118
5.23	Dipole antenna with 2×3 BSR unit cells for positive deflection (a) designed configuration and (b) fabricated	



prototype	119
5.24 Simulated and measured reflection coefficient of the dipole antenna with and without BSR unit cells during the positive deflection	120
5.25 Simulated and measured normalized radiation patterns of the dipole antenna with BSR array in E-plane at 27.7 GHz, 28 GHz, and 28.3 GHz	121
5.26 Simulated and measured gain of the dipole antenna and antenna with BSR array for the positive deflection angle	121
5.27 Radiation power flow of the dipole antenna in E-plane at 28 GHz (a) without BSR (b) with BSR	122
5.28 Dipole antenna with 2×3 BSR unit cells for negative deflection, (a) designed configuration and (b) fabricated prototype	122
5.29 Simulated and measured reflection coefficient of the dipole antenna with and without BSR unit cells during the negative deflection	123
5.30 Simulated and measured normalized radiation patterns of the dipole antenna with BSR array in E-plane at (a) 27.7 GHz, (b) 28 GHz and (c) 28.3 GHz	124
5.31 Simulated and measured gains of the dipole antenna and antenna with BSR for negative tilt	125
5.32 Radiation power flow of the dipole antenna in E-plane at 28 GHz (a) without BSR (b) with BSR	125
6.1 (a) Schematic view of the proposed antenna, (b) photo of prototype front layer, and (c) photo of prototype back layer	129
6.2 The results of simulation and measurement of the proposed antenna (a) reflection coefficient, and (b) normalized radiation pattern	129
6.3 Two mediums with different refractive indices in the way of electromagnetic rays	131



6.4	(a) the designed structure of the proposed antenna with ASSR array for negative deflection, and (b) fabricated antenna	132
6.5	Reflection coefficient of the proposed antenna and antenna with ASSR metamaterial array (negative tilt angle)	133
6.6	Normalized radiation patterns of a proposed antenna loaded by ASSR array (negative tilt angle)	133
6.7	Simulated and measured gain of the dipole antenna and metamaterial antenna (negative tilt angle)	134
6.8	Impact of the metamaterial array's width on the radiation pattern (negative tilt angle)	135
6.9	(a) The designed structure of the proposed antenna with ASSR array for positive tilt, and (b) fabricated antenna	135
6.10	Reflection coefficient of the proposed antenna with and without ASSR array (positive tilt angle)	136
6.11	Normalized simulated and measured radiation patterns of a printed dipole antenna with ASSR array (positive tilt angle)	136
6.12	Simulated and measured gain of the dipole antenna and metamaterial (positive tilt angle)	137
6.13	Impact of the metamaterial array width on the antenna's radiation pattern (positive tilt angle)	138
6.14	The configuration of the bow-tie antenna	139
6.15	Front and back layers of the fabricated antenna	140
6.16	Measured and simulated reflection coefficient of the proposed antenna	141
6.17	Simulation and measurement results of radiation patterns (a) E-plane, and (b) H-plane	141
6.18	Method of radiation pattern deflection using two metamaterial configurations in the way of electromagnetic rays	142



6.19	Configuration of the bow-tie antenna loaded by metamaterial array (a) positive deflection, and (b) negative deflection	144
6.20	Simulated reflection coefficients of the proposed antenna loaded by metamaterial (a) positive deflection and (a) negative deflection	145
6.21	Simulated radiation patterns of the proposed antenna with metamaterial array in E-plane at 3.5 GHz	146
6.22	Simulated normalized radiation patterns of the proposed antenna with metamaterial array in H-plane at 3.5 GHz	146
6.23	Simulated gain of the bow-tie antenna and antenna with SSR array	147
6.24	Fabricated metamaterial antenna (a) positive deflection angle and (b) negative deflection angle	147
6.25	Simulated and measured reflection coefficients of the bow-tie antenna loaded by SSRs (a) positive deflection, and (b) negative deflection	148
6.26	Simulated and measured radiation patterns of the bow-tie antenna loaded by SSRs in E-plane at 3.5 GHz	148
6.27	Simulated and measured radiation patterns of the bow-tie antenna loaded by SSRs in H-plane at 3.5 GHz	149
6.28	Simulated and measured gain of the antenna and antenna with SSRs	149
6.29	Metamaterial antenna (a) arrangement of PIN diodes in the front layer (b) bias lines and vias in the back layer of structure	150
6.30	Reflection coefficient of the antenna and antenna loaded by SSRs (a) positive deflection (b) negative deflection	152
6.31	Simulated radiation patterns of the bow-tie antenna with SSRs for both deflection angles in E-plane at 3.5 GHz	153



- 6.32 Simulated radiation patterns of the bow-tie antenna with SSRs for both deflection angles in H-plane at 28 GHz 153
- 6.33 The photograph of the fabricated metamaterial bow-tie antenna reconfigured by PIN diodes (a) front layer (b) back layer 154
- 6.34 Reflection coefficient of the antenna and antenna loaded by metamaterial (a) positive deflection, and (b) negative deflection 155
- 6.35 Simulation and measurement results of the radiation patterns for positive and negative deflection angles in E-plane at 3.5 GHz 156
- 6.36 Simulation and measurement results of the radiation patterns for positive and negative deflection angles in H-plane at 3.5 GHz 156



LIST OF SYMBOLS AND ABBREVIATIONS

LHM	Left-handed material
DNG	Double negative material
NRI	Negative refractive index
MMW	Millimetre-wave
EIT	Electromagnetically induced transparency
5G	Fifth-generation
QoS	Quality of service
BFN	Beam-forming network
ADS	Advance design system
DSRR	Modified double square ring resonator
CSR	Contiguous squares resonator
BSR	Bridge shape resonator
ASSR	Adjacent square-shaped resonator
SSR	Split squares resonator
4G	Fourth generation
THz	Terahertz
TW	Thin-wire
SRR	Split ring resonator
CSRR	Complementary split ring resonator
DPS	Double positive material
ENG	Epsilon negative
MNG	Mu-negative
DNG	Double-negative
ASRR	Asymmetric split range resonator
DSRR	Double-gap split ring resonator
MEMS	Micro-electro-mechanical systems
DBS	Double bowknot shaped structure

EBG	Electromagnetic band gap
CSSRR	Circular spiral split ring resonator
SHR	Semi H-shaped resonator
HIS	High impedance surface
AMC	Artificial magnetic conducting
FL-LHM	Folded-line left-handed
DSR	Double split rectangular
CST	Computer Simulation Technology
PCB	Printed circuit board
FDTD	Finite-difference-time-domain
FEM	Finite-element method
AF	Array factor
UV	Ultra-violet
EM	Electromagnetic wave
PEC	Perfect electric conducting
PMC	Perfect magnetic conducting



PTTA UTHM
PERPUSTAKAAN TUNKU TUN AMINAH

LIST OF APPENDICES

APPENDIX	TITLE	PAGE
A	List of Publications and Awards	177
B	Rogers RT5880 Datasheet	180
C	MA4AGFCP910 Diode Datasheet	182
D	BAR50 02V Diode Datasheet	186
E	Equivalent Circuit Calculations	191



PTTA UTHM
PERPUSTAKAAN TUNKU TUN AMINAH

CHAPTER 1

INTRODUCTION

1.1 Introduction

Metamaterials are artificially engineered materials with unique electromagnetic response not found in natural materials. In the last two decades, these materials have attracted much attention because of their extraordinary electromagnetic characteristics such as negative permittivity and permeability, and thereby negative index of refraction [1][2]. Victor Veselago proved the theoretical basis of the negative permittivity and permeability properties in 1968. Three decades later, the negative behaviour was verified experimentally by Smith in 2000 [3][4]. By exploiting these unique electromagnetic characteristics, metamaterials can be utilized as a part of numerous essential applications such as super-lenses, cloaking technology, and design and enhance antenna performance [5]. Metamaterials are usually referred to as double-negative (DNG) material, negative refractive index (NRI) material, or left-handed material (LHM). In the LHM, both of permittivity and permeability are negative while both of them are positive in the right-handed material (RHM).

The study of the metamaterial characteristics has been improved through several strategies and procedures. Nonetheless, few problems had been encountered, such as the small bandwidth and inherent losses that restrict the spectrum and the variety of their applications. Metamaterials experience high losses, particularly when the operation frequency is increased to the higher range, such as in the millimeter-wave (MMW) spectrum [6]. These inherent losses can have negative impacts on the performance of the unnatural electromagnetic properties of the metamaterials.

Metamaterial losses are induced by two components, which are radiation losses (i.e. Metamaterial structure scatters the electromagnetic wave away from the incident wave) and ohmic losses (i.e. the dissipation energy due to the intrinsic ohmic losses of the conducting layer of the metamaterial structure), where the former is being a major component of such losses [7]. In recent years, the researchers had introduced several approaches to overcome metamaterial losses at different frequency bands, such as tailoring geometry of the metamaterial structure [8], using the electromagnetically induced transparency (EIT) [7], integrating gain materials [9]. Thus, a low-loss metamaterial configuration is in high demand to enhance the performance of metamaterial devices, especially at a high-frequency range.

On the other hand, the most critical trends in the development of electromagnetic devices-based metamaterials are to design multi-function and miniaturized structures that can be achieved by reconfiguring these artificial materials. In recent years, reconfigurable metamaterials received considerable attention since they exhibit a variable response to an incident electromagnetic waves, thereby increasing the functionality of such structures [10]. This property gives the designers a wide degree of freedom for the synthesis of innovative adaptive systems. The reconfigurable metamaterials have found applications in fabricating reconfigurable antennas [11]. In particular, these materials can enhance the propagation properties of the antenna system, such as scanning range and directivity while simultaneously reducing cost and size.

The type of application and its importance in the area of wireless communication is an essential part of the antenna design. The rapid increase in the number of wireless service users has created severe challenges for telecommunications industries regarding bandwidth scarcity in current networks. Therefore, service providers have moved toward fifth-generation (5G) networks to meet these requirements. 5G is a modern communication standard which is proposed to enhance the current communication standards. 5G networks provide data rates of up to 1000 times higher and bandwidth 10 times greater than current communication networks. The unlicensed spectrum below 6 GHz (3.5 GHz) band and MMW band have been proposed recently to deliver 5G for their advantages such as large bandwidth, which translates directly to higher data transfer rates and low latency, reducing the interference and increasing the frequency reuse factor [12][13]. The 5G networks would exploit the enormous amount of spectrum in the MMW bands to

greatly increase communication capacity and to resolve the spectrum crowding problem in the current communication networks [14]. A few bands of the MMW spectrum have been assigned for the 5G networks, such as 28 GHz, 38 GHz, 60 GHz, 71–76 GHz and 81–86 GHz band. Nevertheless, these frequencies experience a very high propagation loss according to Friis' formula, thereby providing short-range communications compared to the currently used bands [15]. For the smoother achievement of 5G technology in the early stage and to alleviate the propagation loss introduced by MMW, the telecommunications operators plan to employ the existing base station sites at sub-6 GHz of 3.5 GHz band [16]. The sub-6 GHz of 3.5 GHz is the candidate for early deployment of 5G networks across the globe at microwave regime with benefits of low propagation loss compared to MMW regime and wide bandwidth of 400 MHz [17][18]. In fact, this frequency band has a notable free space path loss over the currently used bands, and this issue can be mitigated using a directional antenna with enhanced gain [19]. The high gain directional antenna can be obtained by loading reconfigurable metamaterial structures into planar antennas.

Today, the advanced communication systems supply us with different functionalities such as high transmission rate, multi-band performance, and many services. However, these systems should be at a low price, robust, and simple to use. These features show that if an individual system can perform multiple functions, the cost and complexity of the system can be decreased significantly. The antenna design is an indivisible part of any communication system, and the development of this part can have a notable impact on the overall performance of the communication system. Thus, applying reconfigurable antennas that can provide variety at different levels is an encouraging solution to improve the communication system. By adjusting the radiated fields of the effective aperture of the antenna, the reconfigurable property of an antenna can be achieved [20][21]. In this regard, antenna currents are redistributed, which leads to change in the antenna's functionalities. This change in functions empowers the designers to introduce reconfigurable antennas for various wireless communication platforms. Many reports had been carried out on different kinds of reconfiguration, including the frequency reconfigurable, radiation pattern reconfigurable, directivity reconfigurable, and polarization reconfigurable [22]. In the literature, various approaches had been proposed to perform the reconfiguration, such as mechanical, thermal, and electronic. However, it is needless to say that electronic reconfiguration is the most interesting method because of their significant

applications in modern communication systems. Recently, reconfigurable antennas can be achieved by integrating reconfigurable metamaterials. This integration can enhance the propagation properties of the antenna [23].

This research is conducted to design, fabricate, and measure low loss metamaterial structures. Then, the metamaterial structures are reconfigured using the electronic approach based PIN diode for providing different refractive indices. After that, reconfigurable metamaterial structures are loaded into planar dipole and bow-tie antennas to perform the beam-tilting capability at two different 5G bands of 28 GHz and 3.5 GHz. This approach is considered among the best candidates to reconfigure the planar antennas for its advantages over conventional methods such as compact size, separable reconfigurable part, ease of implementation, the possibility of integration in the same substrate of the antenna, and enhancing the gain through the reconfiguration process.

1.2 Motivation

The explosive growth in the wireless communication system motivates the researchers to investigate different ways of boosting the current cellular network standards. The cellular network generations are assessed by the increase in the user devices, traffic data, and the demand for a better quality of service (QoS) [24][25]. By the end of 2020, there are expectations of increasing the connected devices up to 50 billion [26]. As a result, the massive growths in the data traffic and spectral scarcity have become noticeable problems. The 5G wireless networks are the following telecommunication standard, which proposed to enhance the performance of the current networks. The spectrum shortage is a critical problem for 5G wireless networks. To overcome this issue, the unlicensed spectrum below 6 GHz and MMW had been proposed to deliver 5G mobile network because of their large bandwidth. The MMW bands, such as the 28 GHz, the 38 GHz, the 60 GHz, and the E-band (71–80 GHz), are the essential bands that are investigated recently by the researchers to deliver 5G mobile networks.

The MMW communications experience a very high propagation loss compared to other communication systems that use a low operation frequency, which in turn limits their promising applications. These losses are inherently due to the rain

attenuation and atmospheric and molecular absorption characteristics of MMW propagation [27]. To mitigate this issue, the MMW communications are used for indoor environments with small cell sizes on the order of 200 m. Moreover, directional high gain antennas are employed at both the transmitter and receiver terminals of the system. On the other hand, the sub-6 GHz of 3.5 GHz band is proposed recently as a candidate band for future 5G networks. The telecommunications operators can utilize the present base station sites at 3.5 GHz frequency band to deliver 5G with low free space path loss and a large bandwidth of 400 MHz. However, this band has a noticeable propagation loss, which can be compensated using a directional antenna with enhanced gain [19]. Therefore, antennas with beam deflection and gain enhancement capability are in high demand to support 5G communication systems.

In this thesis, the MMW band of 28 GHz has been chosen to be the operation band of the reconfigurable metamaterial antenna. This band offers a low rain attenuation and oxygen absorption in comparison with the other MMW bands, such as 60 GHz [28]. Moreover, the pattern reconfigurable metamaterial antenna has been designed at the sub-6 GHz of 3.5 GHz band due to the low path loss and large bandwidth. Few works had been carried out to discuss the integrating of metamaterials with the antenna system for deflecting the radiated beam toward the desired direction at the microwave spectrum. However, these works experience several shortcomings, such as the large profile structure, fixed and small beam deflection angle, provide a beam deflection only in one direction, and drop in the gain. This motivates us to propose novel geometric shapes of metamaterial structures, which provide significantly low losses as compared to that of the various reported metamaterial structures. Further, the reconfigurable metamaterial structures are integrated with printed dipole and bow-tie antennas for beam deflection application at two different frequency bands of 28 GHz and 3.5 GHz.

1.3 Problem statement

Many challenges affect the implementation of metamaterial-based devices, including narrow bandwidth and losses. These impairments restrict the spectrum and the variety of their applications. Metamaterials experience high losses, especially when

the frequency is increased to the higher range, such as the MMW frequency range. Consequently, the losses can have negative influences and adverse effects on the realization of the unique electromagnetic properties of the metamaterials. A novel and modified geometric shapes of metamaterials with relatively low loss are in high demand to exploit the unique electromagnetic properties and enable metamaterial-based devices at the high-frequency range [29].

Pattern reconfigurable antenna is essential for a terminal with an array of antennas such as the base station that arranges to direct the radiation pattern under the horizon to cover the small cells. Deflecting an antenna's radiation pattern in a predefined direction is very important for enhancing the performance of communication systems in terms of the quality of service, system security, avoiding interference, and economizing power. Several approaches had been proposed in the literature to redirect the antenna's main beam to the desired direction, such as phased array antenna and adaptive antenna using the beam-forming network. By using these methods, the phase of each element is changed progressively to steer the main beam into the predefined direction. However, they suffer from a complex feeding network, an expensive transceiver system, a large size, and a drop in the gain [30][31]. To overcome these issues, the electronically reconfigurable metamaterial is loaded into the single element planar antenna for achieving beam tilting with advantages over conventional methods, such as adjustable refractive index, the simplicity of implementation, small size structure, and the potential of integration onto the same substrate of the antenna. Moreover, the gain is also enhanced through the reconfiguration process, which in turn helps to alleviate the free space path loss that results from increasing the operating frequency to high-frequency range such as MMW. Reconfigurable metamaterial structure also provides the possibility of designing a separable reconfigurable part that can be attached to or be extracted from the antenna structure as demanded.

1.4 Objectives

The main objectives of this research are:

- I. To design, fabricate, and measure metamaterial structures with low loss property operating at the MMW spectrum.
- II. To simulate and analyze the reconfigurable refractive index metamaterial structure for MMW and sub-6 GHz spectrums.
- III. To design, fabricate, and experiment a 5G planar antenna based on reconfigurable metamaterial structure operating at two different frequency bands of 28 GHz (MMW) and 3.5 GHz (sub-6 GHz) for 5G beam deflection applications.

1.5 Scopes of the research

The main aim of this research is to propose different shapes of the metamaterials with relatively low loss property. After that, these metamaterial structures are reconfigured and integrated with planar single element antenna for 5G beam deflection applications at two different frequency bands of 28 GHz (MMW) and 3.5 GHz (sub-6 GHz). The significant research scopes are as follows:

- I. Study and understand the concept and classifications of metamaterials. Investigate the types and effects of the metamaterial impairments, i.e. the losses. Also, review the techniques used for compensation these losses. Accordingly, propose metamaterial structures operating at MMW with losses less than 0.5 dB. Moreover, propose an equivalent circuit model to predict the behaviour of the metamaterial structures. The CST microwave studio and advanced design system (ADS) had been utilized to simulate the proposed structures and equivalent circuit, respectively.
- II. Study and investigate the techniques that are used to reconfigure the metamaterials. Hence, an electronic approach-based PIN diode is proposed to achieve reconfigurable metamaterials at MMW and microwave spectrums. In this regard, different metamaterial structures are reconfigured at both frequency bands to meet the requirements of this study of creating different refractive index values. The reconfigurable structures are implemented in the simulation stage using two methods, which are the copper strip to mimic the dimensions of a real PIN diode and the S-parameters of the real PIN diode.

- III. Design, fabricate and measure the dipole and bow-tie antennas that operate at two different 5G bands of 28 GHz and 3.5 GHz. Then, these antennas are integrated with reconfigurable metamaterial. This integration between the two antennas and reconfigurable metamaterials leads to deflect the main beam of the proposed antennas in both positive and negative directions. Furthermore, the gain is improved through the deflection process, thereby alleviating the free space path loss and increasing the reliability of the communication system.
- IV. Finally, analysis, discussion, and comparison between simulation and measurement results. Then writing the final report.

1.6 Research structure outline

A brief introduction to metamaterials and their applications in antenna fields, motivation, problem statement, the scope of research and research objectives are presented in Chapter 1. Figure 1.1 shows the steps of the thesis outline.

In Chapter 2, the history of the metamaterials and their applications in antenna fields are discussed. Previously reported works of the different techniques used to reduce the metamaterial loss are described in detail. Also, the well-known methods of reconfigurable metamaterials are investigated, and their performance is compared. Further, the different types of reconfigurable antennas had been discussed. The review focused on the reconfigurable radiation pattern. The integration of metamaterials with the antenna for beam deflection applications is discussed and reviewed for different antenna configurations and frequency bands.

In Chapter 3, the research methodology is presented. The general steps of the research are provided in the form of a flow chart. The two stages of this research are discussed in detail. The first stage is to design and simulate the metamaterial structures and metamaterial antennas. The validation of the simulation results is investigated in the second stage, in which the fabrication and measurement are discussed in detail.

Chapter 4 is divided into two main stages. In the first stage, five metamaterial structures are proposed to operate at both MMW and microwave spectrums with low

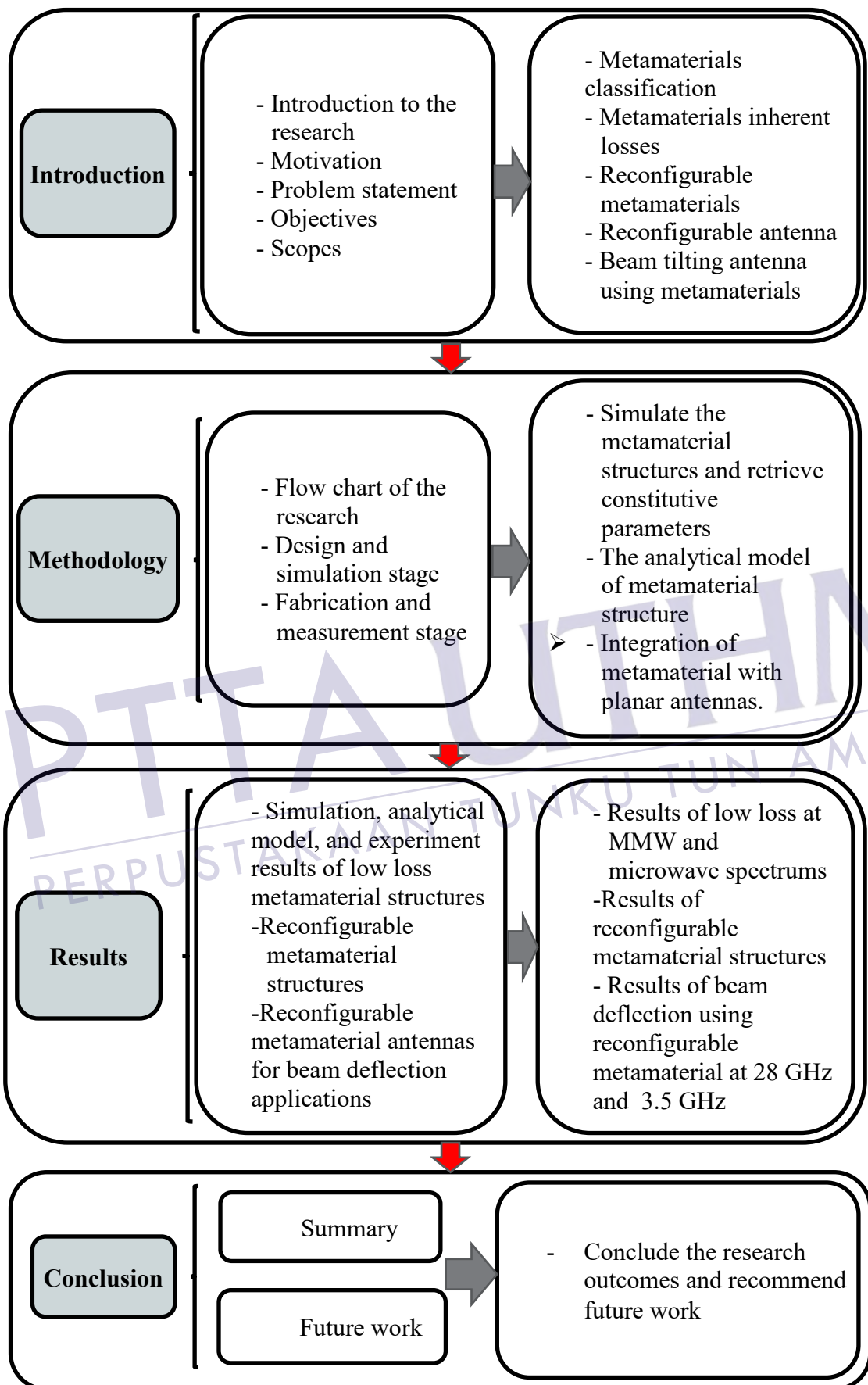


Figure 1.1: The steps of the thesis outline.

loss, including the modified double square ring resonator (DSRR), contiguous squares resonator (CSR), bridge shaped resonator (BSR), adjacent square-shaped resonator (ASSR), and split square resonator (SSR). The losses of all proposed structures are studied. In the second stage, the CSR, BSR, SSR structures have been reconfigured to achieve different refractive index values, which are used in Chapters 5 and 6 for beam deflection applications. Further, the equivalent circuit model of the metamaterial structures is introduced, in which the LC equivalent circuit model is used to predict the electromagnetic behaviour of the proposed structures.

In Chapter 5, the beam deflection antenna is proposed using different metamaterial structures at a 5G candidate band of 28 GHz. The dipole antenna is investigated numerically and experimentally at 28 GHz. Reconfigurable CSRs is included into the proposed antenna for beam deflection application. The CSR array has the capability for deflecting the main beam in both directions, positive and negative. Moreover, the gain is enhanced through the deflection process. Another structure, BSR, is also embedded into the proposed antenna for achieving higher deflection angles with gain enhancement in both directions.

In Chapter 6, two metamaterial structures are used to tilt the main beam of the dipole and bow-tie antennas at a 5G candidate band of 3.5 GHz. The dipole and bow-tie antennas are investigated numerically and experimentally at 3.5 GHz. ASSR array is added to the dipole antenna for tilting the main beam with gain enhancement in both positive and negative directions. On the other hand, the reconfigurable SSRs are integrated with the bow-tie antenna to produce high deflection angles with gain enhancement in both directions. Both passive and active reconfigurable metamaterial antennas have been fabricated and measured to validate the simulated results.

In Chapter 7, the conclusion of the research and the recommendations for future work are introduced.

CHAPTER 2

LITERATURE REVIEW

2.1 Introduction

Metamaterials researches have attracted widespread interest in recent years due to their unnaturally electromagnetic response—in particular, negative refraction index and left-handed propagation. Metamaterials, with their unusual properties that cannot be found in nature, have shown tremendous potential in many fields of science and technology. Since the beginning of this century, metamaterials had presented innovative solutions to overcome the restrictions and challenges of conventional microwave components and had been extensively utilized in many antenna applications [32].

The study of the unique electromagnetic properties of metamaterials has been boosted through several strategies and approaches. Nonetheless, few impairments had been encountered, such as the inherent losses and narrow bandwidth that restrict the spectrum and the variety of their applications. The existence of the metamaterial losses primarily limits the performance of the metamaterials. In the microwave frequency region, these losses are acceptable and the unique electromagnetic properties of the metamaterials can still be obtained. However, metamaterials experience very high losses during the increase of the frequency to the higher range, such as the MMW spectrum [6]. At a high-frequency range, these losses have a significant impact on the unusual electromagnetic characteristics of the metamaterials. There are two components of metamaterial losses namely radiation and ohmic losses [7]. Metamaterial elements scatter the electromagnetic energies

away from the incident wave, thereby inducing the radiation loss. On the other hand, ohmic loss arises from the metallic layer of the metamaterial structures.

In the literature, various potential approaches had been proposed for defeating the problem of high losses in metamaterials. However, in these present solutions, either it cannot be applied at high-frequency bands, or the extraordinary response of the metamaterial cannot be preserved [33]. Hence, new metamaterial structures with relatively low loss are in high demand. To overcome the major components of these losses and to enhance the performance of the devices based on metamaterials at the high-frequency range, the EIT phenomenon and tailoring the equivalent circuit parameters for obtaining a high L/C ratio are used to explain the low loss property in the proposed metamaterial structures.

Recently, researchers focused on the metamaterial design which leads to the realization of reconfigurable property [34][35]. Reconfigurable metamaterials are designed for controlling electromagnetic waves using conventional reconfigurable approaches such as mechanical, thermal and electronic. A noticeable variation in the electric and magnetic response was observed when the geometry of the unit cell is rearranged [36]. Reconfigurable metamaterials present enormous opportunities to achieve different technologies such as beam-switching, imaging, and optimizing the scattering (transmission, reflection, and absorption) of the material.

On the other hand, 5G is the next telecommunication standard which proposed as highly needed to enhance the existence fourth-generation (4G) telecommunication networks in terms of high speed, availability of large bandwidth, broad channel capacity, high quality and low latency [12]. The advance in the wireless telecommunications networks such as 5G should be turned into smart antenna systems. It is essential to dynamically deflect the radiation of the antennas for enhancing the quality of service, system security, avoiding interference, and economizing power. In the literature, many approaches had been proposed to guide the antenna's main beam toward a specific direction. These include phased array antenna and adaptive antenna using the beam-forming network (BFN) [37][38]. Nonetheless, these approaches suffer a complex feeding network, an expensive transceiver system, a large size, and a fixed scanning angle.

In recent studies, the conventional metamaterial structures are integrated with the planar antenna for beam tilting applications. This approach has advantages over conventional beam deflection methods, including adjustable refractive index, the

simplicity of implementation, small size structure, the potential of integration onto the same substrate of the antenna, and gain enhancement. Considerable work had been carried out to deploy metamaterials for beam-steering applications by integrating metamaterials in the front of the individual planar antenna. This integration creates different refractive indices mediums in the vicinity of the proposed antenna, thereby deflecting the radiation beam in the desired direction. Moreover, unlike other methods, the gain is improved through the deflection process [39][40].

2.2 Metamaterials

2.2.1 History

The prefix "Meta" is taken from Greek, which means "beyond ". The novel and desired macroscopic properties of the metamaterial are beyond the naturally occurring materials. The first significant contribution to the metamaterial was declared in 1968 by Victor Veselago [3]. He stated that the negative permittivity and negative permeability of the material would be possible theoretically. Three decades later, the first left-handed metamaterial was verified experimentally by Smith. Since the experimental validation of the metamaterial by Smith in 2000, the research in this field has evolved at different frequency ranges, including microwave spectrum [41], terahertz spectrum [42][43], optical spectrum [44][45] and MMW spectrum [46][47].

The conventional design of the metamaterial is composed of Thin-Wire (TW) structure that offers a negative value of permittivity ϵ and the Split Ring Resonator (SRR) with a negative value of permeability μ as shown in Figure 2.1 [48][41]. Subsequently, different types of artificial metamaterial unit cells with different shapes had been proposed, including the SRRs and complementary CSRRs [49], broad-side coupled SRRs [50], omega-shaped resonator [51], and S-shaped resonator [52].

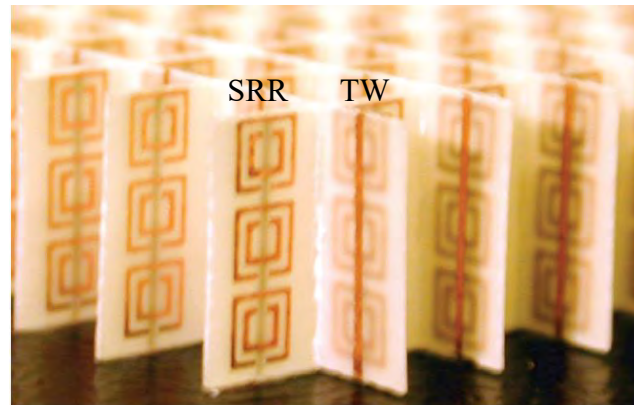


Figure 2.1: Conventional array of metamaterials, TW structure exhibits $(-\epsilon)$ and SRR provides $(-\mu)$ [41].

2.2.2 Metamaterial applications

The potential applications of metamaterials are still being revealed since the possibility of achieving materials not found in nature for different applications is almost limitless. However, the uncommon electromagnetic properties of the metamaterials enable many practical applications in the microwave, MMW wave, and terahertz regimes such as perfect and superlens [53][54], subwavelength resolution and focusing [55], achieving transparency by cloaking technologies [56], scattering suppression [57], and enhance nonlinear phenomenon [58]. In spite of remarkable features of metamaterials in altering the constitutive parameters of the material, the resonant nature of metamaterials remains an unsolved dilemma, which leads to high losses and narrow bandwidth impairments that restrict their applications in many aspects.

2.2.3 Metamaterial classifications

In conventional materials, the propagation of the electromagnetic wave is influenced by their refractive index. The electromagnetic characteristics of a metamaterial can be expressed by Lorentz dispersive model with two frequency-dependent macroscopic parameters, permittivity $\epsilon(\omega)$ and permeability $\mu(\omega)$ as follows:

$$\varepsilon(\omega) = 1 + \frac{\omega_{pe}^2}{\omega_{Te}^2 - \omega^2 - i\omega\gamma_e} \quad (2.1)$$

$$\mu(\omega) = 1 + \frac{\omega_{pm}^2}{\omega_{Tm}^2 - \omega^2 - i\omega\gamma_m} \quad (2.2)$$

where the ω_{Te} and ω_{Tm} are the transverse resonance frequency. ω_{pe} and ω_{pm} are the electric and magnetic coupling strengths. γ_e and γ_m are the parameters of the absorption.

Figure 2.2 shows the classifications of the material, which includes all types of materials according to their electromagnetic properties. The top-right quarter depicts that materials of both permittivity and permeability are positive, which covers most conventional dielectric materials. The epsilon negative (ENG) material is shown in the top-left quarter which depicts a negative permittivity at some

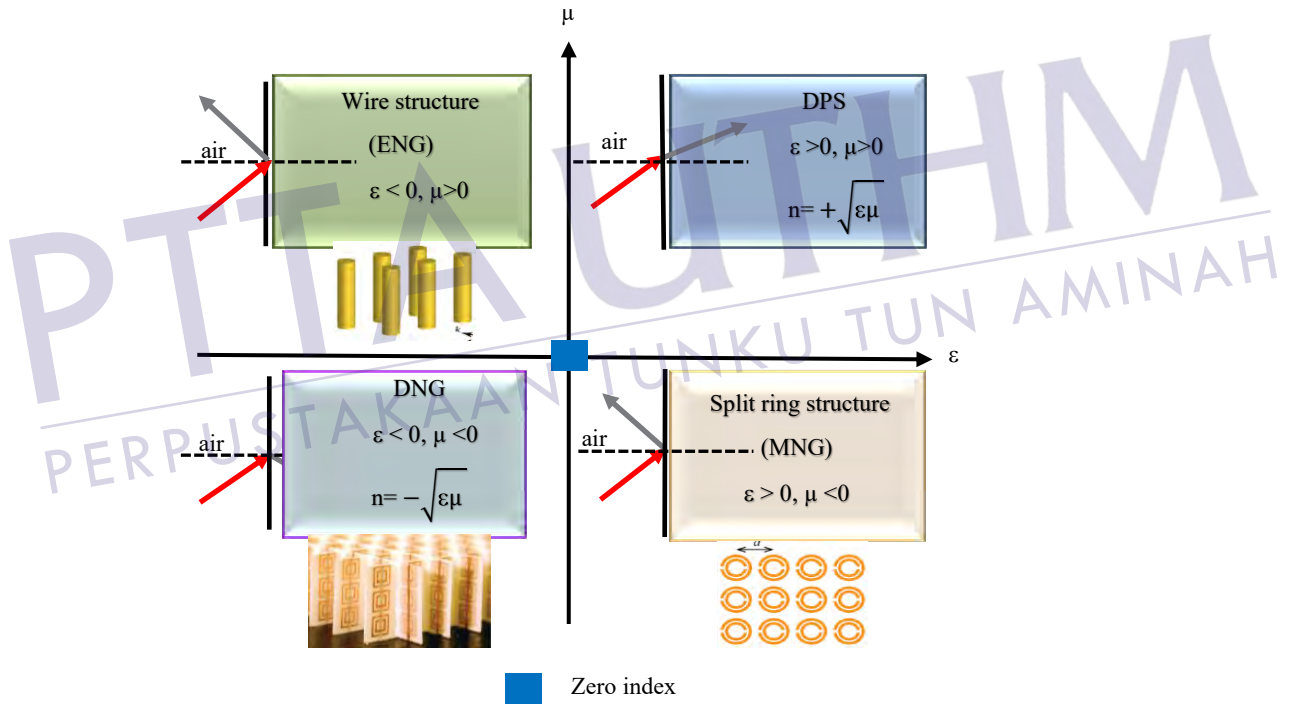


Figure 2.2: Classifications of the mediums based on permittivity and permeability with the electromagnetic wave interacting with four possible materials.

frequencies and positive permeability at other frequencies. This type of material can be achieved by periodic wire structures [48]. The first human-made material with negative permeability is presented in the bottom-right quarter which is called a mu-negative (MNG) material. This type of material is performed by a periodic structure of SRRs [41]. The bottom-left quarter is the most interesting one, in which permittivity and permeability are simultaneously negative and it is known as double-

negative (DNG) metamaterial. No such material can be found in nature. The origin of Figure 2.2 can be classified as zero-index material where ϵ and μ are at zero or approaching zero. The electromagnetic wave interacts with the four materials as shown in Figure 2.2. It can be seen that the electromagnetic wave normally refracted for double-positive (DPS) material. The electromagnetic wave does not propagate in the MNG and ENG materials. On the other hand, the metamaterials refracted the waves away from normal. In this research, different metamaterial structures had been proposed at the MMW spectrum and microwave spectrum. The constitutive parameters of these structures had been reconstructed using a well-known method. The losses of these structures had investigated, especially at the MMW spectrum. After that, these structures are reconfigured to achieve different refractive indices, which are used to deflect the main beam of the proposed antennas at two different 5G bands.

2.2.4 Refractive index of the metamaterials

The capability to control the macroscopic electromagnetic characteristics, particularly the permittivity, permeability and refractive index by modifying the geometry and combination of the incorporated elements leads to the number of essential material designs and applications [59]. Most important amongst these is material with negative index refraction. The incident waves (evanescent waves) of the positive refractive index material suffer a significant decay while the negative refractive index materials enhance these waves. Negative refractive index metamaterials, which were verified experimentally at the beginning of this century, are mostly engineered materials consisted of electric and magnetic structures that have negative permittivity and negative permeability at a specific frequency range [60]. The direction of the energy flow of electromagnetic waves is described by the Poynting, \vec{S} . The \vec{S} is expressed as follows:

$$\vec{S} = \vec{E} \times \vec{H} \quad (2.3)$$

where \vec{E} and \vec{H} are the electric and magnetic fields, respectively. In the right-handed material (RHM), both of ϵ and μ are positive. The electric field \vec{E} , magnetic field \vec{H} , and wave vector, \vec{k} , follow the right-hand rule. In this case, the \vec{S} and \vec{k} have the same

direction. On the other hand, the backward-wave propagation is observed when both ε and μ are negative. In this case, the \vec{S} has the opposite direction with respect to \vec{k} . In other words, the phase velocity and group velocity are anti-parallel. In this case, the slab is a LHM, and the left-hand rule can be expressed as follows:

$$\vec{S} = -\vec{E} \times \vec{H} \quad (2.4)$$

The mathematical expression of the negative refraction can be achieved when both ε and permeability μ are negative, as follows:

$$n = \sqrt{\varepsilon \times \mu} \quad (2.5)$$

The permittivity and permeability in terms of magnitude and phase are expressed as follows:

$$\varepsilon = |\varepsilon|e^{j\Phi_e}, \mu = |\mu|e^{j\Phi_h} \quad (2.6)$$

where the Φ_e and Φ_h are any values between the 0 and π . To obtain a negative index of refraction, both of them are supposed to be π .

$$n = \sqrt{\varepsilon \times \mu} e^{j\frac{1}{2}(\Phi_e + \Phi_h)} \quad (2.7)$$

where $e^{j\pi} = -1$

$$n = -\sqrt{\varepsilon\mu} \quad (2.8)$$

The first negative refractive index (NRI) is introduced by conventional metamaterial of cut wire and SRR structures. The main shortcomings of this traditional metamaterial are that the bandwidth is too tight and the losses are high at the high-frequency range, which restricts their promising applications as absorbers, imaging resolution, and an invisibility cloak [61].

2.3 Metamaterial loss

One of the significant challenges that face the researchers in the metamaterials field is the inherent losses at different frequency spectrums. These losses are usually caused by the metallic layer of the structure and radiation scattering. The losses seriously limit the practical applications of the metamaterials, which are also a major obstacle in the design of efficient metamaterial devices such as absorbers and an

invisibility cloak. The metal used in the metallic layers of the metamaterial structure behaves in a less than ideal manner, especially at high frequencies such as MMW and optical regimes. Thus, the intrinsic or ohmic loss is a very crucial issue and needs to be addressed especially at high-frequency range [62]. The intrinsic loss can be defined as the total power absorbed by the metamaterial due to resistive heating of the metallic layers of the structure.

The inherent losses of the metamaterial are not limited to the metal loss of the structure. The design of the metamaterial can bring substantial loss effects, and these losses can be classified into two types: resonant losses [63] and radiation losses [64]. The resonance losses are induced by increasing the operating frequency of the metamaterial unit cells. On the other hand, the radiation loss which is the dominant component of the losses, is due to the metamaterial elements that scatter the electromagnetic waves away from the incident wave. The inherent losses caused by ohmic and radiation losses are explained in Figure 2.3. The metamaterial receives the incident electromagnetic wave from an external source. Part of the incident wave is dissipated inside the metamaterial through the equivalent ohmic resistance resulting from the metallic layers of the structure. Another part of the incident wave, which is the larger, radiates off the metamaterial, thereby inducing the radiation losses. To measure the metamaterial losses, various factors have been used such as transmission coefficient and surface current distribution [6]. The transmission loss, S_{21} , is used to measure the peak of the transmission band of the metamaterial at the desired frequency.

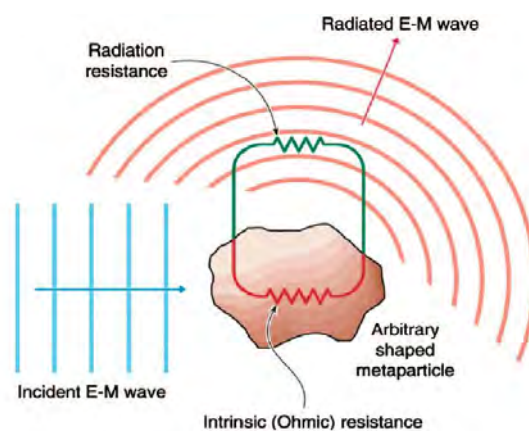


Figure 2.3: The inherent losses in metamaterials [7].

On the other hand, if the surface current distribution is not uniform over the metamaterial metallic layers, the magnetic dipole moment and the electric dipole moment are excited, thereby inducing the radiation losses. Thus, to design a low loss metamaterial structure, the structure should have a proper geometrical arrangement with uniform surface current distribution. Several techniques were extensively reported in the literature to compensate losses in the metamaterials. The most common techniques are using the principal of the EIT and tailoring the geometry of metamaterial structures.

2.3.1 Electromagnetically induced transparency (EIT)

EIT is an appealing physical phenomenon and defined as a quantum interference effect that occurs in the three-level atomic system, in which an opaque atomic medium is introduced to be transparent in the extremely narrowband window within a broad absorption spectrum [65]. EIT effect can be achieved in the metamaterials field. However, this effect can only be induced passively by tailoring the geometrical parameters of the resonator structures [65] [66]. To date, EIT is the most effective approach for compensating the metamaterial losses. By applying the principle of EIT, metamaterial structure induces opposite current directions resulting in the destructive interference of the scattering fields, and thus suppression the radiation loss. In the last decade, various metamaterial structures based on EIT phenomenon are reported to reduce the loss. This physical phenomenon provides substantially reduction in the metamaterial loss at different frequency regimes from microwave [67] to terahertz [64]. At a higher frequency range, metamaterial losses are less discussed in the literature so far, and this work is considered among the first to investigate these inherent losses at the MMW spectrum.

In the literature, most of the reports discussed the losses of the SRR which considers the conventional structure of the metamaterials. Hai-ming Li et al. in [67] reported a low loss EIT metamaterial-based electric toroidal dipolar response. This response is induced by currents flowing on the surface of a torus along its meridians. The metamaterial structure is composed of asymmetric split range resonator (ASRR) that acts as electric toroidal dipolar response and cut wire represents the electric

response as illustrated in Figure 2.4. The transmission dip band has appeared at 8.12 GHz. The destructive interference between the ASRR and cut wire results in a high

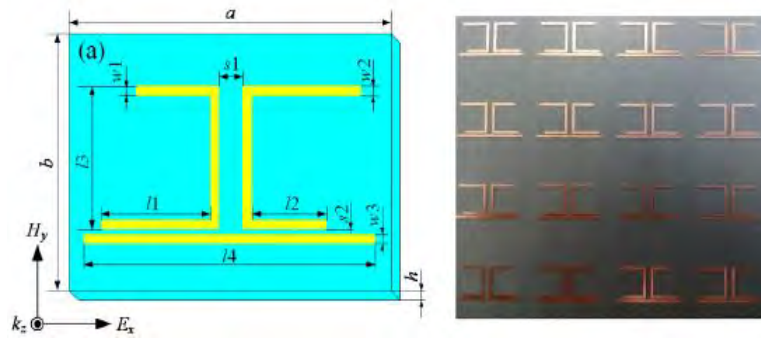


Figure 2.4: Schematic view of the structure and the fabricated prototype.

transparency peak at 8.12 GHz. Due to break in the symmetry of the structure, there is a freedom in the coupling between two modes which helps in reducing the loss of the structure. The ASRR and cut wire unit cell achieved a very low loss of 0.56 dB (0.88 in the linear scale). The overall dimensions of the unit cell are $0.43 \lambda_o \times 0.43 \lambda_o$ at 8.12 GHz, where λ_o refers to the free space wavelength at the resonance frequency. Although the EIT had been induced at low frequency, the loss of the structure is still high. In [68], the authors proposed two mirrored double-gap splitting resonator SRRs and cut wire shapes to induce EIT, as shown in Figure 2.5. The

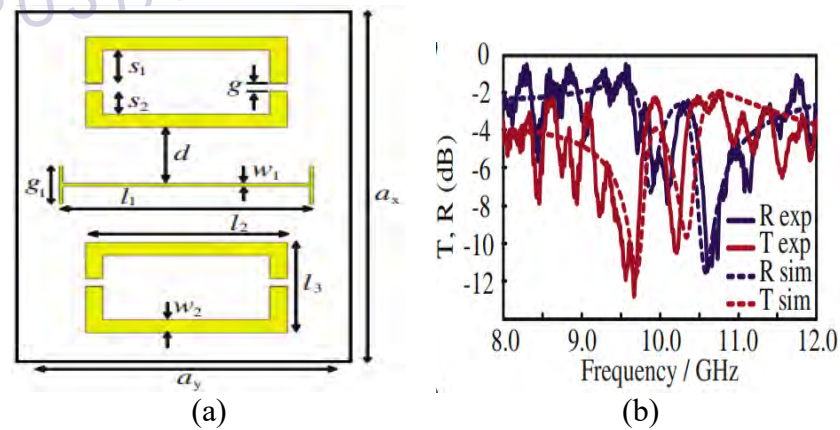


Figure 2.5: (a) Schematic view of SRRs and cut wire, and (b) simulated and measured transmission and reflection coefficients.

electric and magnetic fields are induced by the cut wire and SRRs, respectively. This design provided a loss of about 2.5 dB (0.56 in the linear scale) at 10.05 GHz with dimensions of $0.7 \lambda_o \times 0.4 \lambda_o$. Although the symmetry of the structure was retained

through the inducing of EIT and the unique properties of metamaterials can still be achieved within the microwave regime, the proposed structure induces a high loss at the resonant frequency. Also, the loss of conventional SRR had been studied and compensated based on EIT phenomena in [69]. The unit cell structure was composed of two SRRs with wide and narrow dimensions that were exploited to exhibit a low loss behavior. Figures 2.6 (a) and (b) depict the periodic structure with single unit cell geometry and the transmission coefficient, respectively. The proposed structure achieved a low loss of 0.5 dB (0.89 in the linear scale) at 5.5 GHz. The low loss property is investigated in terms of transmission coefficients, constitutive parameters, and surface current. The physical size of the structure is $0.3 \lambda_o \times 0.3 \lambda_o$. Nevertheless, the loss remains high at the microwave regime. The losses of conventional SRRs and I-shape cut wire had been investigated and reduced using the EIT phenomenon in [70]. The schematic view of SRRs and I-shape cut wire unit cell and its fabricated prototype are illustrated in Figure 2.7. This structure produced a low loss of 0.97 dB (0.8 in the linear scale) at 5.41 GHz. The main advantage of this design is the low-profile structure where the dimensions of the structure are $0.3 \lambda_o \times 0.2 \lambda_o$. This size is small in comparison with other reported literature. The loss at the high-frequency range is discussed based on EIT in [71]. The unit cell is composed of a double-gap split ring resonator (DSRR) and a straight metallic strip. The authors optimize the coupling between the two shapes to reduce the loss. The proposed structure achieves a transmission peak of 3 dB (0.5 in the linear scale) at 500 GHz.

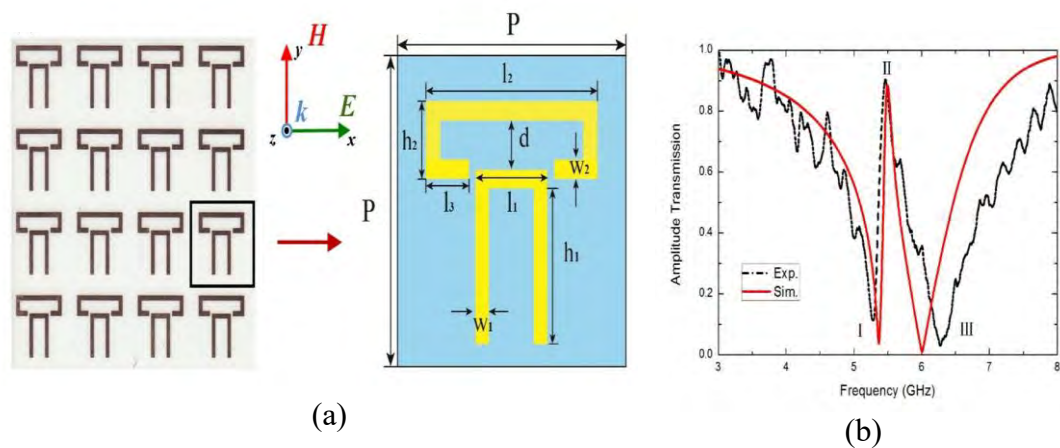


Figure 2.6: (a) The periodic structure with a single unit cell geometry, and (b) simulated and measured transmission and reflection coefficients.

The proposed structure has a physical size of $0.4 \lambda_o \times 0.4 \lambda_o$. However, the loss is still quite high.

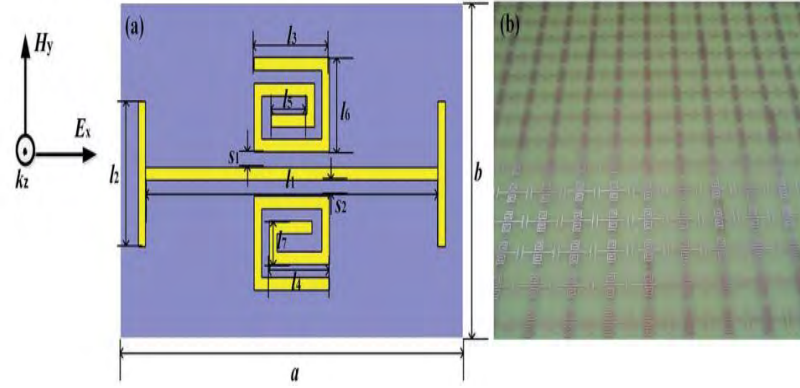


Figure 2.7: (a) Schematic view of SRRs and I-shape cut wire, and (b) fabricated prototype.

2.3.2 Tailoring geometry of metamaterials

The metamaterial loss restricts the applications of such exotic materials and delays incorporating them in the practical devices unless efficient ways of reducing them are found. As mentioned previously, the EIT with destructive interference of the scattering fields is the most common method to achieve low loss property. It is worth of mentioning that there are other methods proposed in the literature to reduce the loss, such as the tailoring geometry of the metamaterial structures. This method is performed by optimizing the structure parameters through the simulation to exhibit a low loss property.

The authors in [72] investigated the losses by using a double bowknot shaped structure (DBS). The overall dimension of the DBS unit cell is $0.3 \lambda_o \times 2.7 \lambda_o$ at 11 GHz. The overlap between the electric and magnetic resonance had been exploited to achieve a low loss structure. By optimizing the structural parameters, three types of DBS (A, B, and C) with small losses were introduced. The losses based on transmission peak are 2.75 dB (0.53 in the linear scale), 2.3 dB (0.59 in the linear scale), and 1.33 dB (0.74 in the linear scale) for type A, type B, and type C, respectively. Another approach based on tailoring geometry is by exploiting the structure parameters L and C . In the RLC circuit, the losses rely on the Q factor and the parameters of the circuit, where the Q -factor is given by $Q = (I/R) \times \sqrt{L/C}$. The

decrease in the capacitance, C values or the increase in the inductance, L values causes an increase in the Q-factor value, thereby reducing the circuit losses. The authors in [63] and [73] propose fishnet and circular spiral split ring resonator (CSSRR) to exhibit a low loss property, respectively. The parameters of both structures were optimized through the simulation to increase the L/C ratio, thereby increasing the Q-factor and reducing the losses. The asymmetrically aligned paired cut wires on both sides of the cyclo-olefin Polymer substrate is proposed in [74] to provide low loss at 0.42 THz. By optimizing the cut wire structure from symmetry to asymmetry, the structure loss was reduced to 0.91 dB (0.81 in the linear scale). In [75], the authors reported a near-zero-index metamaterial-based S-shaped with wires on the surface and through the substrate. The proposed structure offered a low loss in the wide frequency range at X-band. The bandwidth and loss were mainly controlled by the surface wire width, in which the electric plasma frequency and the magnetic plasma frequency can be adjusted. The broadband low loss of 1.7 dB (0.67 in the linear scale) was obtained in the wide frequency range from 10.72 GHz to 11.4 GHz. Table 2.1 summarizes the recent literature of the metamaterial loss reduction using different reduction mechanisms.

Table 2.1: Summary of previous reports on metamaterial loss reduction.

Ref.	Metamaterial shape (physical size)	Frequency band	Transmission peak (the losses)	Reduction loss approach	Drawbacks
[67]	ASRR and cut wire ($0.43\lambda_o \times 0.43\lambda_o$)	Microwave regime 8.12 GHz	0.56 dB (0.88 in the linear scale).	EIT	The loss still high at microwave regime.
[68]	SRRs and cut wire ($0.7\lambda_o \times 0.4\lambda_o$)	Microwave regime 10.05 GHz	2.5 dB (0.56 in the linear scale)	EIT without breaking the symmetry of the structure	The loss is quite high at microwave regime.
[69]	SRR ($0.3\lambda_o \times 0.3\lambda_o$)	Microwave regime	0.5 dB (0.89 in the linear	EIT	The loss remains

		5.5 GHz.	scale)		high at the microwave regime.
[70]	SRRs and I-shape cut wire ($0.3 \lambda_o \times 0.2 \lambda_o$)	Microwave regime 5.41 GHz.	0.97 dB (0.8 in the linear scale)	EIT	Low profile structure, but the loss still high at low frequency range.
[71]	DSRR) and the straight metallic strip ($0.4 \lambda_o \times 0.4 \lambda_o$)	Terahertz regime 0.5 THz.	3 dB (0.5 in the linear scale)	EIT	The loss is still high and discussed in the simulation stage only.
[72]	DBS ($0.3 \lambda_o \times 2.7 \lambda_o$)	Microwave regime 11 GHz.	-Type A= 2.75 dB (0.53 in the linear scale), -Type B= 2.3 dB (0.59 in the linear scale) -Type C= 1.33 dB (0.74 in the linear scale)	Tailoring geometrical structure (optimizing the electric and magnetic resonance)	Three types achieved high losses at microwave regime.
[75]	S-shaped based wires ($0.18 \lambda_o \times 0.11 \lambda_o$)	Microwave regime 10.72-11.4 GHz	1.7 dB (0.67 in the linear scale)	Tailoring geometrical structure (controlling	Although the symmetry is retained,

REFERENCES

- [1] M. T. Islam, A. Hoque, A. F. Almutairi, and N. Amin, "Left-handed metamaterial-inspired unit cell for S-Band glucose sensing application," *Sensors*, vol. 19, no. 1, pp. 1–12, 2019.
- [2] S. Zhang, W. Fan, N. C. Panoiu, K. J. Malloy, R. M. Osgood, and S. R. J. Brueck, "Experimental demonstration of near-infrared negative-index metamaterials.," *Phys. Rev. Lett.*, vol. 95, no. 13, pp. 1–4, 2005.
- [3] V. G. Veselago, "The electrodynamics of substances with simultaneously negative values of ϵ and μ ," *Sov. Phys. Uspekhi*, vol. 10, no. 4, pp. 509–514, 1968.
- [4] D.R. Smith, W.J. Padilla, D.C. Vier, S.C. Nemat-Nasser, and S. Schultz, "Composite medium with simultaneously negative permeability and permittivity," *Phys. Rev. Lett.*, vol. 84, no 18, pp. 4184–4187, 2000.
- [5] J. D. Binion, E. Lier, T. H. Hand, Z. H. Jiang, and D. H. Werner, "A metamaterial-enabled design enhancing decades-old short backfire antenna technology for space applications," *Nat. Commun.*, vol. 10, no. 1, pp. 1–7, 2019
- [6] L. Zhu, F. Y. Meng, L. Dong, J. H. Fu, and Q. Wu, "Low-loss magnetic metamaterial at THz frequencies by suppressing radiation losses," *IEEE Trans. Terahertz Sci. Technol.*, vol. 3, no. 6, pp. 805–811, 2013.
- [7] K. L. Tsakmakidis, M. S. Wartak, J. J. H. Cook, J. M. Hamm, and O. Hess, "Negative-permeability electromagnetically induced transparent and magnetically active metamaterials," *Phys. Rev. B - Condens. Matter Mater. Phys.*, vol. 81, no. 19, pp. 1–11, 2010.
- [8] Y. Fan, Z. Wei, H. Li, H. Chen, and C. M. Soukoulis, "Low-loss and high-Q planar metamaterial with toroidal moment," *Phys. Rev. B - Condens. Matter Mater. Phys.*, vol. 87, no. 11, pp. 1–5, 2013.
- [9] Z. Dong, H. Liu, T. Li, Z. Zhu, S. Wang, J. Cao, S. Zhu, X. Zhang, "Optical loss compensation in a bulk left-handed metamaterial by the gain in quantum dots Optical," *Appl. Phys. Lett.*, vol. 96, no. 4, pp. 1–3, 2010.
- [10] S. Bang, J. Kim, G. Yoon, T. Tanaka, and J. Rho, "Recent advances in tunable and reconfigurable metamaterials," *Micromachines*, vol. 9, no. 11, pp. 560 – 583, 2018.
- [11] J. P. Turpin, J. a. Bossard, K. L. Morgan, D. H. Werner, and P. L. Werner, "Reconfigurable and Tunable Metamaterials: A Review of the Theory and Applications," *Int. J. Antennas Propag.*, vol. 2014, pp. 1–18, 2014.
- [12] S. S. T.S.Rappaport R. Mayzus,H. Zhao, Y.Azar, K.Wang, G.N. Wong, J.K. Schulz, M. Samimi, and F. Gutierrez, "Millimeter wave mobile communications for 5G cellular: It will work!," *IEEE Access*, vol. 1, pp. 335–

349, 2013.

- [13] T. Bai and Heath Jr. Robert W, "Coverage and rate analysis for millimeter wave cellular networks," *IEEE Trans. Wirel. Commun.*, vol. 14, no. 2, pp. 1–33, 2014.
- [14] Y. Niu, Y. Li, D. Jin, L. Su, and A. V. Vasilakos, "A survey of millimeter wave communications (mmWave) for 5G: opportunities and challenges," *Wirel. Networks*, vol. 21, no. 8, pp. 2657–2676, 2015.
- [15] D. Nandi and A. Maitra, "Study of rain attenuation effects for 5G Mm-wave cellular communication in tropical location," *IET Microw., Antennas Propag.*, vol. 12, no. 9, pp. 1504–1507, 2018.
- [16] S. Saxena, B. K. Kanaujia, S. Dwari, S. Kumar, and R. Tiwari, "MIMO antenna with built-in circular shaped isolator for sub-6 GHz 5G applications," *Electron. Lett.*, vol. 54, no. 8, pp. 6–7, 2018.
- [17] Y. L. Ban, C. Li, C. Y. D. Sim, G. Wu, and K. L. Wong, "4G/5G multiple antennas for future multi-mode smartphone applications," *IEEE Access*, vol. 4, pp. 2981–2988, 2016.
- [18] A. Alieldin, Y. Huang, M. Stanley, S. Joseph, and D. Lei, "A 5G MIMO antenna for broadcast and traffic communication topologies based on pseudo inverse synthesis," *IEEE Access*, vol. 6, pp. 65935–65944, 2018.
- [19] A. Dadgarpour, B. Zarghooni, B. S. Virdee, and T. A. Denidni, "Beam-deflection using gradient refractive-index media for 60-GHz end-fire antenna," *IEEE Trans. Antennas Propag.*, vol. 63, no. 8, pp. 3768–3774, 2015.
- [20] N. Ojaroudi Parchin, H. Jahanbakhsh Basherlou, Y.I. Al-Yasir, A. Abdulkhaleq, and R. Abd-Alhameed, "Reconfigurable antennas: switching techniques—A survey," *Electronics*, vol. 9, no. 2, pp. 1–14, 2020.
- [21] N. Ojaroudi Parchin, H. Jahanbakhsh Basherlou, Y. Al-Yasir, R. Abd-Alhameed, A. Abdulkhaleq, and J. Noras, "Recent developments of reconfigurable antennas for current and future wireless communication systems," *Electronics*, vol. 8, no. 2, pp. 1–17, 2019.
- [22] Y. Zhou, R. S. Adve, S. Member, S. V. Hum, and S. Member, "Design and evaluation of pattern reconfigurable antennas for MIMO applications," *IEEE Trans. Antennas Propag.*, vol. 62, no. 3, pp. 1084–1092, 2014.
- [23] S. K. Patel, K. H. Shah, and Y. P. Kosta, "Frequency-reconfigurable and high-gain metamaterial microstrip-radiating structure," *Waves in Random and Complex Media*, vol. 29, no. 3, pp. 523–539, 2019.
- [24] A. Shahmansoori, G. E. Garcia, and G. Destino, "Position and orientation estimation through millimeter wave MIMO in 5G systems," *IEEE Trans. Wirel. Commun.* vol. 17, no. 3, pp. 1822–1835, 2017.
- [25] Y. Zeng, L. Yang, and R. Zhang, "Multi-user millimeter wave MIMO with full-dimensional lens antenna array," *IEEE Trans. Wirel. Commun.*, vol. 17, no. 4, pp. 2800–2814, 2018.
- [26] N. Barreto, B. Faria, E. Almeida, and I. Rodriguez, "5G – wireless communications for 2020," *Journal of Communication and Information Systems*, vol. 31, no. 1, pp. 146–163, 2016.
- [27] O. Semiari, W. Saad, M. Bennis, and B. Maham, "Caching meets millimeter wave communications for enhanced mobility management in 5G networks,"

- IEEE Trans. Wirel. Commun.*, vol. 17, no. 2, pp. 779–793, 2018.
- [28] G. R. Maccartney and S. Member, “Indoor office wideband millimeter-wave propagation measurements and channel models at 28 and 73 GHz for ultra-dense 5g wireless networks,” *IEEE Access*, vol. 3, pp. 2388–2424, 2015.
- [29] M. Kim, and J. Rho, “Metamaterials and imaging,” *Nano Convergence*, vol. 2, no. 1, pp. 1–16, 2015.
- [30] A. Dadgarpour, B. Zarghooni, B. S. Virdee, and T. A. Denidni, “Single End-Fire Antenna for Dual-Beam and Broad Beamwidth Operation at 60 GHz by Artificially Modifying the Permittivity of the Antenna Substrate,” *IEEE Trans. Antennas Propag.*, vol. 64, no. 9, pp. 4068–4073, 2016.
- [31] B. Zarghooni, A. Dadgarpour and T. A. Denidni, “Millimeter-Wave Antenna Using Two-Sectioned Metamaterial Medium,” *IEEE Antennas and Wireless Propagation Letters*, vol. 15, pp. 960–963, 2016.
- [32] N. Engheta and R. W. Ziolkowski, “A positive future for double negative metamaterials,” *IEEE Microw. Theory Tech., Spec. Issue Metamaterials*, April, vol. 4, no. 4, pp. 1535–1556, 2005.
- [33] V. a Fedotov, T. Uchino, and J. Y. Ou, “Low-loss plasmonic metamaterial based on epitaxial gold monocrystal film,” *Opt. Express*, vol. 20, no. 9, pp. 9545–9550, 2012.
- [34] J. Zhu, D. Li, S. Yan, Y. Cai, Q. H. Liu, and T. Lin, “Tunable microwave metamaterial absorbers using varactor-loaded split loops,” *EPL (Europhysics Lett.)*, vol. 112, no. 5, pp. 1–5, 2015.
- [35] L. Ivzhenko, E. Odarenko, and S. I. Tarapov, “Mechanically tunable wire medium metamaterial in the millimeter wave band,” *Progress In Electromagnetics Research*, vol. 64, pp. 93–98, 2016.
- [36] N. I. Zheludev and Y. S. Kivshar, “From metamaterials to metadevices,” *Nat. Mater.*, vol. 11, no. 11, pp. 917–924, 2012.
- [37] P. Deo, D. Mirshekar-syahkal, L. Seddon, S. E. Day, and F. A. Fernández, “60 GHz liquid crystal phased array using reflection-type phase shifter,” *In 7th European Conference on Antennas and Propagation (EuCAP)*, pp. 920–922, 2013.
- [38] H. Chu, Y. Guo, S. Member, and Z. Wang, “60-GHz LTCC wideband vertical off-center dipole antenna and arrays,” *IEEE Trans. Antennas Propag.*, vol. 61, no. 1, pp. 153–161, 2013.
- [39] A. Dadgarpour, B. Zarghooni and T. A. Denidni, “Beamforming bow-tie antenna for millimeter-wave applications using metamaterial lens,” *IEEE International Symposium on Antennas and Propagation & National Radio Science Meeting*, Vancouver, pp. 254–255, 2015.
- [40] A. Dadgarpour and B. Zarghooni, “Enhancement of Tilted Beam in Elevation Plane for Planar End-Fire Antennas Using Artificial Dielectric Medium,” *IEEE Trans. Antennas Propag.*, vol. 63, no. 10, pp. 4540–4545, 2015.
- [41] R. Shelby, D. Smith, and S. Schultz, “Experimental verification of a negative index of refraction,” *Science*, vol. 292, no. 5514, pp. 77–79, 2001.
- [42] T. J. Yen, W.J Padilla, N. Fang, D.C. Vier, D.R. Smith, J.B. Pendry, D.N. Basov, and X. Zhang, “Terahertz magnetic response from artificial materials,” *Science*, vol. 303, no. 5663, pp. 1494–1496, 2004.

- [43] A. K. Azad, J. Dai, and W. Zhang, "Transmission properties of terahertz pulses through subwavelength double split-ring resonators," *Opt. Lett.*, vol. 31, no. 5, pp. 634–636, 2006.
- [44] N. Engheta, "Circuits with light at nanoscales: optical nanocircuits inspired by metamaterials.," *Science*, vol. 317, no. 5845, pp. 1698–1702, 2007.
- [45] M. Soukoulis, Costas M; Linden, Stefan; Wegener, "Negative refractive index at optical wavelengths," *Science*, vol. 315, pp. 47–49, 2007.
- [46] M. Navarro-Cia, M. Beruete, I. Campillo, and M. S. Ayza, "Beamforming by left-handed extraordinary transmission metamaterial Bi- and plano-concave lens at millimeter-waves," *IEEE Trans. Antennas Propag.*, vol. 59, no. 6, pp. 2141–2151, 2011.
- [47] R. Amiri, B. Zarghooni, A. Dadgarpour, J. Pourahmadazar, and T. A. Denidni, "Anisotropic metamaterial unit-cell for millimeter- wave applications," *17th International Symposium on Antenna Technology and Applied Electromagnetics (ANTEM)*, pp. 1–2, 2016.
- [48] J. B. Pendry, A. J. Holden, D. J. Robbins, and W. J. Stewart, "Low frequency plasmons in thin-wire structures," *J. Phys. Condens. Matter*, vol. 10, no. 22, pp. 4785–4809, 1999.
- [49] J. Naqui, S. M. Ieee, M. Durán-sindreu, M. Ieee, and F. Martín, "Modeling split ring resonator (SRR) and complementary split ring resonator (CSRR) loaded transmission lines exhibiting cross polarization effects," *IEEE Antennas Wirel. Propag. Lett.*, vol. 12, pp. 178–181, 2013.
- [50] J. Wang, S. Qu, J. Zhang, H. Ma, Y. Yang, C. Gu, X. Wu, and Z. Xu "Tunable left-handed metamaterial based on modified broadside-coupled split-ring resonators," *Progress In Electromagnetics Research*, vol. 6, pp. 35 – 45, 2009.
- [51] Z. Li, K. Aydin, and E. Ozbay, "Retrieval of effective parameters for bianisotropic metamaterials with omega shaped metallic inclusions," *Photonics Nanostructures - Fundam. Appl.*, vol. 10, no. 3, pp. 329–336, 2012.
- [52] H. Chen, L. Ran, J. Huangfu, X. Zhang, K. Chen, T. M. Grzegorzczuk, and J. A. Kong, "Left-handed materials composed of only S-shaped resonators," *Phys. Rev. E*, vol. 70, no. 5 2, pp. 1–4, 2004.
- [53] S. Haxha, F. AbdelMalek, F. Ouerghi, M. D. B. Charlton, A. Aggoun, and X. Fang, "Metamaterial superlenses operating at visible wavelength for imaging applications," *Sci. Rep.*, vol. 8, no. 1, pp. 1–15, 2018.
- [54] A. Archambault, M. Besbes, and J. J. Greffet, "Superlens in the time domain," *Phys. Rev. Lett.*, vol. 109, no. 9, pp. 1–4, 2012.
- [55] K. Aydin, I. Bulu, and E. Ozbay, "Subwavelength resolution with a negative-index metamaterial superlens," *Appl. Phys. Lett.*, vol. 90, no. 25, pp. 1–3, 2007.
- [56] S. S. Islam, M. M. Hasan, and M. R. I. Faruque, "A new metamaterial-based wideband rectangular invisibility cloak," *Appl. Phys. A Mater. Sci. Process.*, vol. 124, no. 2, pp. 2–6, 2018.
- [57] J. C. Soric, P. Y. Chen, A. Kerkhoff, D. Rainwater, K. Melin, and A. Alù, "Demonstration of an ultralow profile cloak for scattering suppression of a finite-length rod in free space," *New J. Phys.*, vol. 15, no. 3, pp. 1–18, 2013.



- [58] J. B. Pendry, A. J. Holden, D. J. Robbins, and W. J. Stewart, "Magnetism from conductors and enhanced nonlinear phenomena," *IEEE Trans. Microw. Theory Tech.*, vol. 47, no. 11, pp. 2075–2084, 1999.
- [59] B. A. Slovick, "Negative refractive index induced by percolation in disordered metamaterials," *Phy. Rev. B*, vol. 95, no. 9, pp. 1–5, 2017.
- [60] X. Jing, X. Gui, R. Xia, and Z. Hong, "Ultrabroadband unnaturally high effective refractive index metamaterials in the terahertz region," *IEEE Photonics Journal*, vol. 9, no. 1, pp. 1–7, 2017.
- [61] Z. Shen, H. Yang, X. Huang, and Z. Yu, "Design of negative refractive index metamaterial with water droplets using 3D-printing," *Journal of Optics*, vol. 19, no. 11, pp. 1–15, 2017.
- [62] D. Güney, T. Koschny, and C. M. Soukoulis, "Reducing ohmic losses in metamaterials by geometric tailoring," *Phys. Rev. B - Condens. Matter Mater. Phys.*, vol. 80, no. 12, pp. 1–7, 2009.
- [63] J. Zhou, T. Koschny, and C. M. Soukoulis, "An efficient way to reduce losses of left-handed metamaterials," *Opt. Express*, vol. 16, no. 15, pp. 11147–11152, 2008.
- [64] L. Zhu, F. Y. Meng, J. H. Fu, Q. Wu, and J. Hua, "An approach to configure low-loss and full transmission metamaterial based on electromagnetically induced transparency," *IEEE Trans. Magn.*, vol. 48, no. 11, pp. 4285–4288, 2012.
- [65] X. Liu, J. Gu, R. Singh, Y. Ma, J. Zhu, Z. Tian, M. He, J. Han, and W. Zhang, "Electromagnetically induced transparency in terahertz plasmonic metamaterials via dual excitation pathways of the dark mode," *Appl. Phys. Lett.*, vol. 100, no. 13, pp. 1–4, 2012.
- [66] Z. Y. Li, Y. Ma, R. Huang, R. Singh, J. Gu, Z. Tian, J. Han, and W. Zhang, "Manipulating the plasmon-induced transparency in terahertz metamaterials," *Opt. Express*, vol. 19, no. 9, pp. 8912–8919, 2011.
- [67] H. M. Li, S.B. Liu, S.Y. Liu, S.Y. Wang, G.W. Ding, H. Yang, Z.Y. Yu, and H.F. Zhang, "Low-loss metamaterial electromagnetically induced transparency based on electric toroidal dipolar response," *Appl. Phys. Lett.*, vol. 106, no. 8, pp. 1–4, 2015.
- [68] L. Zhang, P. Tassin, T. Koschny, C. Kurter, S. M. Anlage, and C. M. Soukoulis, "Large group delay in a microwave metamaterial analog of electromagnetically induced transparency," *Appl. Phys. Lett.*, vol. 97, no. 24, pp. 1–3, 2010.
- [69] Y. Tian, S. Hu, X. Huang, Z. Yu, H. Lin, and H. Yang, "Low-loss planar metamaterials electromagnetically induced transparency for sensitive refractive index sensing," *J. Phys. D*, vol. 50, no. 40, pp. 1–21, 2017.
- [70] X. JunáHe. and C. HuiáZhao, "A low-loss electromagnetically induced transparency (EIT) metamaterial based on coupling between electric and toroidal dipoles," *RSC Adv.*, vol. 7, no. 88, pp. 55897–55904, 2017.
- [71] Y. Zhang, J. Wu, L. Liang, G. Zhou, F. Zheng, C. Li, C. Zhang, and B. Jin, "Tailoring electromagnetically induced transparency effect of terahertz metamaterials on ultrathin substrate," *Sci. China Inf. Sci.*, vol. 59, no. 4, pp. 1–6, 2016.



- [72] X. Zhou, Y. Liu, and X. Zhao, "Low losses left-handed materials with optimized electric and magnetic resonance," *Appl. Phys. A Mater. Sci. Process.*, vol. 98, no. 3, pp. 643–649, 2010.
- [73] T. Shaw and D. Mitra, "Design of miniaturized , low-loss and flexible multi-band metamaterial for microwave application," *Appl. Phys. A*, vol. 124, no. 4, pp. 1–11, 2018.
- [74] T. A. Suzuki, M. A. Sekiya, T. A. Sato, Y. Uki, and T. Akebayashi, "Negative refractive index metamaterial with high transmission , low reflection , and low loss in the terahertz waveband," *Opt. Express*, vol. 26, no. 7, pp. 8314–8324, 2018.
- [75] J. Ma, X. Zhu, S. Bi, G. Bai, and Z. Hou, "Low-loss near-zero-index metamaterial based on a single board for broadband electromagnetic-wave switches," *Opt. Commun.*, vol. 446, pp. 113–117, 2019.
- [76] K. Fan and W. J. Padilla, "Dynamic electromagnetic metamaterials," *Mater. Today*, vol. 18, no. 1, pp. 39–50, 2015.
- [77] X. Duan, S. Chen, H. Cheng, Z. Li, and J. Tian, "Dynamically tunable plasmonically induced transparency by planar hybrid metamaterial," *Opt. Lett.*, vol. 38, no. 4, pp. 483–485, 2013.
- [78] H. Yuan, B. O. Zhu, and Y. Feng, "A frequency and bandwidth tunable metamaterial absorber in x-band," *J. Appl. Phys.*, vol. 117, no. 17, pp. 1–6, 2015.
- [79] J. Zhao, Q. Cheng, J. Chen, M. Q. Qi, W. X. Jiang, and T. J. Cui, "A tunable metamaterial absorber using varactor diodes," *New J. Phys.*, vol. 15, no. 4, pp. 1–11, 2013.
- [80] B. Belkadi, Z. Mahdjoub, M. L. Seddiki, And M. Nedil, "A selective frequency reconfigurable bandstop metamaterial filter for WLAN applications," *Turkish J. Electr. Eng. Comput. Sci.*, vol. 26, no. 6, pp. 2977–2986, 2018.
- [81] D. Lee, H. Jeong, and S. Lim, "Electronically switchable broadband metamaterial absorber," *Sci. Rep.*, vol. 7, no. 1, pp. 1–10, 2017.
- [82] H. Jeong and S. Lim, "Broadband frequency- reconfigurable metamaterial absorber using switchable ground plane," *Sci. Rep.*, vol. 8, no. 1, pp. 1–9, 2018.
- [83] J. Fang, J. Huang, Y. Gou, and Y. Shang, "Research on broadband tunable metamaterial absorber based on PIN diode," *Opt. - Int. J. Light Electron Opt.*, vol. 200, pp. 1–5, 2020.
- [84] C. P. Ho, P. Pitchappa, Y. S. Lin, C. Y. Huang, P. Kropelnicki, and C. Lee, "Electrothermally actuated microelectromechanical systems based omega-ring terahertz metamaterial with polarization dependent characteristics," *Appl. Phys. Lett.*, vol. 104, no. 16, pp. 1–5, 2014.
- [85] N. O. Parchin, H. J. Basherlou, Y. I. A. Al-Yasir, A. M. Abdulkhaleq, and R. A. Abd-Alhameed, "Reconfigurable antennas: Switching techniques— a survey," *Electronics*, vol. 9, no. 2, pp. 1–14, 2020.
- [86] H. T. Chen, W.J. Padilla, R.D. Averitt, J.F. O'hara and M. Lee, "Active terahertz metamaterial devices," *Nature*, vol. 444, no. 7119, pp. 597–600, 2006.



- [87] X. J. He, T.Y. Li, L. Wang, J.M. Wang, J.X. Jiang, G.H. Yang, F.Y. Meng, and Q. Wu, "Electrically tunable terahertz wave modulator based on complementary metamaterial and graphene," *J. Appl. Phys.*, vol. 115, no. 17, pp. 1–3, 2014.
- [88] B. Zarghooni and T. A. Denidni, "New fractal metamaterial unit-cell for microwave applications," *8th Eur. Conf. Antennas Propagation, EuCAP*, pp. 978–979, 2014.
- [89] S. H. Zainud-deen, M. M. Badawy, and H. A. Malhat, "Reconfigurable transparent all - dielectric water-based metamaterial for microstrip patch antenna gain," *Wirel. Pers. Commun.*, vol. 111, no. 1, pp. 1–5, 2019.
- [90] Y. Zheng, J. Gao, Y. Zhou, X. Cao, H. Yang, S. Li, and T. Li, "Wideband gain enhancement and rcs reduction of fabry-perot resonator antenna with chessboard arranged metamaterial superstrate," *IEEE Trans. Antennas Propag.*, vol. 66, no. 2, pp. 590–599, 2018.
- [91] X. Gao, L. Dai, and A. M. Sayeed, "Low RF-complexity technologies to enable millimeter-wave MIMO with large antenna array for 5G wireless communications," *IEEE Commun. Mag.*, vol. 56, no. 4, pp. 211–217, 2018.
- [92] F. Guidolin, M. Nekovee, L. Badia, and M. Zorzi, "A study on the coexistence of fixed satellite service and cellular networks in a mmWave scenario," in *IEEE International Conference on Communications*, pp. 2444–2449, 2015.
- [93] L. Kong, M. K. Khan, F. Wu, G. Chen, and P. Zeng, "Millimeter-wave wireless communications for IoT-cloud supported autonomous vehicles: Overview, design, and challenges," *IEEE Commun. Mag.*, vol. 55, no. 1, pp. 62–68, 2017.
- [94] A. Pedross-Engel, D. Arnitz, J.N. Gollub, O. Yurduseven, K.P. Trofatter, M.F. Imani, T. Sleasman, M. Boyarsky, X. Fu, D.L. Marks, and D.R. Smith, "Orthogonal coded active illumination for millimeter wave, massive-MIMO computational imaging with metasurface antennas," *IEEE Trans. Comput. Imaging*, vol. 4, no. 2, pp. 184–193, 2018.
- [95] Y. Niu, Y. Li, D. Jin, L. Su, and A. V Vasilakos, "A survey of millimeter wave communications (mmWave) for 5G : opportunities and challenges," *Wireless networks*, vol. 21, no. 8, pp. 2657–2676, 2015.
- [96] S. A. A. Shah, E. Ahmed, M. Imran, and S. Zeadally, "5G for vehicular communications," *IEEE Commun. Mag.*, vol. 56, no. 1, pp. 111–117, 2018.
- [97] J. Gozalvez, T. Generation, and P. Project, "5G Worldwide Developments," *IEEE Veh. Technol. Mag.*, vol. 12, no. 1, pp. 4–11, 2017.
- [98] A. I. Sulyman, A. T. Nassar, M. K. Samimi, and G. R. M. Jr, "Radio propagation path loss models for 5G cellular networks in the 28 GHz and 38 GHz millimeter-wave bands," *IEEE Commun. Mag.*, vol. 52, no. 9, pp. 78–86, 2014.
- [99] Y. J. Guo and P. Qin, "Advances in reconfigurable antenna systems facilitated by innovative technologies," *IEEE access*, vol. 6, pp. 5780–5794, 2018.
- [100] L. Ge, Y. Li, J. Wang, C. Sim, and S. Member, "A Low-profile reconfigurable cavity-backed slot and radiation pattern agility," *IEEE Trans. Antennas Propag.*, vol. 65, no. 5, pp. 2182–2189, 2017.
- [101] F. Zadehparizi, "Increasing reliability of frequency- reconfigurable antennas,"

- IEEE Antennas Wireless Propag. Lett.*, vol. 17, no. 5, pp. 920–923, 2018.
- [102] N. Flaum, C. G. Christodoulou, J. Costantine, J. Woodland, and Y. Tawk, “Reconfigurable antenna system with a movable ground plane for cognitive radio,” *IET Microwaves, Antennas Propag.*, vol. 8, no. 11, pp. 858–863, 2014.
 - [103] J. Row and Y.H. Wei, “Wideband reconfigurable crossed-dipole antenna with quad-polarization diversity,” *IEEE Trans. Antennas Propag.*, vol. 66, no. 4, pp. 2090–2094, 2018.
 - [104] T. Debogovic, and J. Perruisseau-Carrier, “Low loss MEMS-reconfigurable 1-Bit reflectarray cell with dual-linear polarization,” *IEEE Trans. Antennas Propag.* vol. 62, no. 10, pp. 5055–5060, 2014.
 - [105] J. Zhu, B. Peng, and S. Li, “Cavity-backed high-gain switch beam antenna array for 60-GHz applications,” *IET Microwaves, Antennas Propag.*, vol. 11, no. 12, pp. 1776–1781, 2017.
 - [106] D. K. Karmokar, K. P. Esselle, S. G. Hay, and S. Member, “Fixed-frequency beam steering of microstrip leaky-wave antennas using binary switches,” *IEEE Trans. Antennas Propag.*, vol. 64, no. 6, pp. 2146–2154, 2016.
 - [107] S. Chen, P. Qin, W. Lin, and Y. J. Guo, “Pattern-reconfigurable antenna with five switchable beams in elevation plane,” *IEEE Antennas Wireless Propag. Lett.*, vol. 17, no. 3, pp. 454–457, 2018.
 - [108] V. V. Khairnar, B. V. Kadam, C. K. Ramesha, and L. J. Gudino, “A reconfigurable parasitic antenna with continuous beam scanning capability in H-plane,” *AEU - Int. J. Electron. Commun.*, vol. 88, pp. 78–86, 2018.
 - [109] H. Moghadas and M. Daneshmand, “MEMS-tunable half phase gradient partially reflective surface for beam-shaping,” *IEEE Trans. Antennas Propag.*, vol. 63, no. 1, pp. 369–373, 2014.
 - [110] S. Zhang, X. Chen, I. Syrytsin, and G. F. Pedersen, “A Planar switchable 3-D-coverage phased array antenna and its user effects for 28-GHz mobile terminal applications,” *IEEE Trans. Antennas Propag.*, vol. 65, no. 12, pp. 6413–6421, 2017.
 - [111] Y. Zhao, C. Huang, A.-Y. Qing, and X. Luo, “A Frequency and pattern reconfigurable antenna array based on liquid crystal technology,” *IEEE Photonics J.*, vol. 9, no. 3, pp. 1–7, 2017.
 - [112] Y. Garbovskiy, V. Zagorodnii, P. Krivosik, J. Lovejoy, and R. E. Camley, “Liquid crystal phase shifters at millimeter wave frequencies,” *J. Appl. Phys.*, vol. 111, no. 5, pp. 1–4, 2012.
 - [113] Y. Cao, K.S. Chin, W. Che, W. Yang, and E.S. Li, “A Compact 38 GHz multibeam antenna array with multifolded butler matrix for 5G applications,” *IEEE Antennas Wireless Propag. Lett.*, vol. 16, pp. 2996–2999, 2017.
 - [114] F. Costa, S. Member, A. Monorchio, S. Member, and S. Talarico, “An active high impedance surface for low profile tunable and steerable antennas,” *IEEE Antennas Wireless Propag. Lett.*, vol. 7, pp. 676–680, 2008.
 - [115] I. Kim and Y. Rahmat-Samii, “Beam-tilted dipole-EBG array antenna for future base station applications,” *IEEE Antennas Propag. Soc. AP-S Int. Symp.*, pp. 1224–1225, 2013.
 - [116] Y. F. Cao and X. Y. Zhang, “A wideband beam steerable slot antenna using artificial magnetic conductors with simple structure,” *IEEE Trans. Antennas*

- Propag.*, vol.66, no. 4, pp. 1685–1694, 2018.
- [117] A. Artemenko, A. Maltsev, A. Mozharovskiy, A. Sevastyanov, V. Ssorin, and R. Maslennikov, “Millimeter-wave electronically steerable integrated lens antennas for WLAN / WPAN applications,” *IEEE Trans. Antennas Propag.*, vol. 61, no. 4, pp. 1665–1671, 2013.
 - [118] M. W. P. A. N. Systems, K. Hosoya, N. Prasad, K. Ramachandran, N. Orihashi, and S. Kishimoto, “Multiple Sector ID capture (MIDC): A novel beamforming technique for 60-GHz band,” *IEEE Trans. Antennas Propag.*, vol. 63, no. 1, pp. 81–96, 2015.
 - [119] Y. Liu, C. Liu, X. Jin, B. Zhang, Y. Zhang, X. Zhu, B. Su, and X. Zhao, “Beam steering by using a gradient refractive index metamaterial planar lens and a gradient phase metasurface planar lens,” *Microw. Opt. Technol. Lett.*, vol. 60, no. 2, pp. 330–337, 2018.
 - [120] T. A. Dadgarpour, B. Zarghooni, T. A. Denidni and A. A. Kishk, “Dual-band radiation tilting endfire antenna for WLAN applications,” *IEEE Antennas Wirel. Propag. Lett.*, Vol. 15, pp.1466–1469, 2015.
 - [121] H. Barati, M. H. Fakheri, and A. Abdolali, “Experimental demonstration of metamaterial-assisted antenna beam deflection through folded transformation optics,” *J. Opt. (United Kingdom)*, vol. 20, no. 8, pp. 1–11, 2018.
 - [122] M. T. Le, Q. C. Nguyen, and T. P. Vuong, “Design of High-Gain and Beam Steering Antennas Using a New Planar Folded-Line Metamaterial Structure,” *Int. J. Antennas Propag.*, vol. 2014, pp. 1–16, 2014.
 - [123] A. Dadgarpour, B. Zarghooni, B. S. Virdee, and T. A. Denidni, “Beam tilting antenna using integrated metamaterial loading,” *IEEE Trans. Antennas Propag.*, vol. 62, no. 5, pp. 2874–2879, 2014.
 - [124] A. Dadgarpour, A. A. Kishk, and T. A. Denidni, “Dual band high-gain antenna with beam switching capability,” *IET Microwaves, Antennas Propag.*, vol. 11, no. 15, pp. 2155–2161, 2017.
 - [125] Z. Wani, M. P. Abegaonkar, and S. K. Koul, “Millimeter-wave antenna with wide-scan angle radiation characteristics for MIMO applications,” *Int. J. RF Microw. Comput. Eng.*, vol. 29, no. 5, pp. 1–9, 2019.
 - [126] X. Chen, T. M. Grzegorzczuk, B. I. Wu, J. Pacheco, and J. A. Kong, “Robust method to retrieve the constitutive effective parameters of metamaterials,” *Phys. Rev. E.*, vol. 70, no. 1, pp. 1–7, 2004.
 - [127] D. R. Smith and S. Schultz, “Determination of effective permittivity and permeability of metamaterials from reflection and transmission coefficients,” *Phys. Rev. B*, vol. 65, no. 19, pp. 1–5, 2001.
 - [128] A. N. Vicente and C. Junqueira, “The step by step development of NRW method,” *In SBMO/IEEE MTT-S International Microwave and Optoelectronics Conference (IMOC 2011)*, pp. 738–742, 2011.
 - [129] Y. Shi, Z. Li, L. Li, and C. Liang, “An electromagnetic parameters extraction method for metamaterials based on phase unwrapping technique,” *Waves in Random and Complex Media*, vol. 26, no. 4, pp. 417– 433, 2016.
 - [130] K. U. Bae, H. Kim, Y. Kim, and W. Yang, “Improvement of FDTD method regarding cloaking metamaterials by interpolation,” *Journal of Electromagnetic Waves and Applications*, vol. 30, no. 10, pp. 1366–1379,



2016.

- [131] M. Hasan, "Beam steering of eye shape metamaterial design on dispersive media by FDTD method," *International Journal of Numerical Modelling: Electronic Networks, Devices and Fields*, vol. 31, no. 5, pp. 1–12, 2018.
- [132] C. Ding, L. Hao, X. Zhao, C. Ding, L. Hao, and X. Zhao, "Two-dimensional acoustic metamaterial with negative modulus," *J. Appl. Phys.*, vol. 108, no. 7, pp. 1–5, 2010.
- [133] H. Xiong, M. Tang, M. Li, D. Li, and Y. Jiang, "Equivalent circuit method analysis of graphene-metamaterial (GM) absorber," *Plasmonics*, vol. 13, no. 3, pp. 857–862, 2018.
- [134] F. Rao, Z. Yu, X. Huang, S. Hu, Y. Jin, and H. Yang, "Metamaterial-inspired rotation sensor based on complementary single split-ring resonator (CSSRR)," *J. Electromagn. Waves Appl.*, vol. 32, no. 13, pp. 1664–1674, 2018.
- [135] N. Pekçokgüler, G. Dündar, H. Torun, and A. D. Yalç, "A novel equivalent circuit model for split ring resonator with an application of low phase noise reference oscillator," *Integration*, vol. 61, pp. 160–166, 2018.
- [136] V. Torres and F. Falcone, "Equivalent circuit of the double-fishnet metamaterial," *In IEEE Antennas and Propagation Society International Symposium (APSURSI)*, pp. 1364–1365, 2013.
- [137] M. M. Hasan, M. R. I. Faruque, S. S. Islam, and M. T. Islam, "A new compact double-negative miniaturized metamaterial for wideband operation," *Materials*, vol. 9, no. 10, pp. 1–12, 2016.
- [138] P. Yasar-Orten, E. Ekmekci, and G. Turham-Sayan "Equivalent circuit models for split-ring resonator arrays," *PIERS Proceedings*, pp. 534–547, 2010.
- [139] Z. Yonggang, W. U. Jingbo, L. Lanju, and Z. Gaochao, "Effect of loss and coupling on the resonance of metamaterial : An equivalent circuit approach," *Science China Information Sciences*, vol. 57, no. 12, pp. 1–8, 2014.
- [140] S. Ghosh, S. Member, K. V. Srivastava, and S. Member, "An equivalent circuit model of fss based metamaterial absorber using coupled line theory," *Antennas Wireless Propag. Lett.*, vol. 14, pp. 511–514, 2014.
- [141] T. Zhang, W. Xiong, B. Zhao, J. Shen, C. Qiu, and X. Luo, "Equivalent circuit analysis of ‘ U ’ -shaped split ring resonators," *Journal of Modern Optics*, vol. 62, no. 11, pp. 901–907, 2015.
- [142] M.A. Bueno and A.K.T. Assis , "A new method for inductance calculations," *Journal of Physics D: Applied Physics*, vol. 28, no. 9, pp. 1802–1806, 1995.
- [143] S. Li, W. Yu, A. Z. Elsherbeni, W. Li, and Y. Mao, "A novel dual-band left-handed metamaterial design method," *Int. J. Antennas Propag.*, vol. 2017, pp. 1–8, 2017.
- [144] O. G. Vendik and S. P. Zubko, "Modeling and calculation of the capacitance of a planar capacitor containing a ferroelectric thin film," *Technical Physics*, vol. 44, no. 4, pp. 349–355, 1999.
- [145] P. Wang and Z. Cai, "A Compact Ultra-wideband planar printed Bow-Tie quasi-yagi antenna with rhombus director and tapered cps connection structure," *IETE Journal of Research*, vol. 64, no. 3, pp. 324–330, 2018.
- [146] Y. Lin and S. Tsai, "Analysis and design of broadside-coupled striplines-fed Bow-Tie antennas," *IEEE Trans. Antennas Propag.*, vol. 46, no. 3, pp. 459–



460, 1998.

- [147] S. X. Ta, H. Choo, and I. Park, "Broadband printed-dipole antenna and Its arrays for 5G applications," *Antennas Wireless Propag. Lett.*, vol. 16, pp. 2183–2186, 2017.
- [148] A. Munir, S. Aviolanda, and E. Bharata, "Wideband printed dipole antenna fed using modified planar marchand balun," *In International Electronics Symposium (IES)*, pp. 295–298, 2016.
- [149] R. Islam, S. Member, M. Ali, and S. Member, "Elevation plane beam scanning of a novel parasitic array radiator antenna for 1900 MHz mobile handheld terminals," *IEEE Trans. Antennas Propag.*, vol. 58, no. 10, pp. 3344–3352, 2010.
- [150] K. Aydin, E. Cubukcu, E. Ozbay, and M. Bayindir, "Transmission and reflection properties of composite metamaterials in free space," *Conf. Lasers Electro-Optics (CLEO)*, pp. 2592–2595, 2003.
- [151] M. Shahidul Islam, M. Samsuzzaman, G. K. Beng, N. Misran, N. Amin and M. T. Islam, "A Gap Coupled Hexagonal Split Ring Resonator Based Metamaterial for S-Band and X-Band Microwave Applications," *IEEE Access*, vol. 8, pp. 68239–68253, 2020.
- [152] C. H. Zhang, J. B. Wu, B. B. Jin, Z. M. Ji, L. Kang, W. W. Xu, J. Chen, M. Tonouchi, and P. H. Wu., "Low-loss terahertz metamaterial from superconducting niobium nitride films," *Opt. Express*, vol. 20, no. 1, pp. 42–47, 2012.
- [153] T.G. Ma, and S.K. Jeng, "A printed dipole antenna with tapered slot feed for ultrawide-band applications," *IEEE Trans. Antennas Propag.*, vol. 53, no. 11, pp. 3833–3836, 2005.
- [154] W.A. Al Garidi, N.B.M. Sahar, and R. Teymourzadeh, "Planar dipole antenna design at 1800MHz band using different feeding methods for GSM application," *in 10th IEEE International Conference on Semiconductor Electronics (ICSE)*, pp. 560–564, 2012.
- [155] N. A. Malek, S. A. Karsin, S. Y. Mohamad, F. N. M. Isa, A. L. Asnawi, and A. M. Ramly, "Design of a dual band printed dipole antenna for WIFI application," *Journal of Telecommunication, Electronic and Computer Engineering (JTEC)*, vol. 9, no. 4, pp. 63–68, 2017.
- [156] R.A. Alhalabi and G.M. Rebeiz, "High-gain Yagi-Uda antennas for millimeter-wave switched-beam systems," *IEEE Trans. Antennas Propag.*, vol. 57, no. 11, pp. 3672–3676, 2009.
- [157] T. Hongnara, S. Chaimool, P. Akkaraekthalin, and Y. Zhao, "Design of compact beam-steering antennas using a metasurface formed by uniform square rings," *IEEE Access*, vol. 6, pp. 9420–9429, 2018.
- [158] A. C. Durgun, S. Member, C. A. Balanis, L. Fellow, C. R. Birtcher, and D. R. Allee, "Design , simulation , fabrication and testing of flexible Bow-Tie antennas," *IEEE Trans. Antennas Propag.*, vol. 59, no. 12, pp. 4425–4435, 2011.
- [159] S. Eom, Y. Seo, and S. Lim, "Pattern switchable antenna system using inkjet-printed directional Bow-Tie for bi-direction sensing applications," *Sensors*, vol. 15, no. 12, pp. 31171–31179, 2015.



- [160] H. A. Majid, M. K. A. Rahim, M. R. Hamid, and M. F. Ismail, "Frequency and pattern reconfigurable slot antenna," *IEEE Trans. Antennas Propag.*, vol. 62, no. 10, pp. 5339–5343, 2014.



PTTA UTHM
PERPUSTAKAAN TUNKU TUN AMINAH